The dual capture of As^V and As^{III} by UiO-66 and analogues

Cornelius O. Audu, [a] Huong Giang T. Nguyen, [a] Chih-Yi Chang, [a] Michael J. Katz, [a] Lily Mao, [a] Omar K. Farha, [a,b,*] Joseph T. Hupp, [a,*] and SonBinh T. Nguyen [a,*]

[a]Department of Chemistry and International Institute for Nanotechnology, Northwestern University, 2145 Sheridan Road, Evanston, Illinois 60208-3113, USA

[b]Department of Chemistry, Faculty of Science, King Abdulaziz University, Jeddah 22254, Saudi Arabia

Table of Content

S1. Materials and Methods

Unless otherwise stated, all reagents were used as received. Hydrochloric acid, zirconium chloride, and terephthalic acid were purchased from Aldrich Chemicals Company, Inc. (Milwaukee, WI). Concentrated sulfuric acid and glacial acetic acid were purchased from VWR Scientific, LLC (Chicago, IL). Arsenic, zirconium, and sulfur ICP standards were purchased from Sigma-Aldrich Co. LLC (St. Louis, MI). 2,5-Dimercaptoterephthalic acid was prepared using the previously reported protocol.[S1] Ultrapure deionized water (18.2 MΩ cm resistivity) was obtained from a Millipore system (EMD Millipore, Billerica, MA). Solvents were purchased from either Sigma-Aldrich Co. LLC (St. Louis, MI), Fisher Scientific, Inc. (Pittsburg, PA), or Avantor Performance Materials, Inc. (Center Valley, PA) and used as received. All the gases used for the adsorption and desorption measurements were ultra-high purity grade 5 and were obtained from Airgas Specialty Gases (Chicago, IL)

Powder X-ray diffraction (PXRD) patterns were recorded on a Rigaku X-ray Diffractometer Model ATX-G (Rigaku Americas, The Woodlands, TX) equipped with an 18 kW Cu rotating anode, an MLO monochromator, and a high-count-rate scintillation detector. Measurements were made over the range $2° < 2\theta < 40°$ in 0.05° step width with a 2°/min scanning speed.

N$_2$ adsorption and desorption isotherms were measured on a Micromeritics Tristar II 3020 (Micromeritics, Norcross, GA) at 77 K. Before each run, samples were activated at 100-150 °C for 24 h (or until outgass rate ≤ 0.02 mmHg) under high vacuum on either a MasterPrep (Quantachrome Instruments, Boynton Beach, FL) or a Smart VacPrep (Micromeritics, Norcross, GA). At least 50 mg of sample was used in each measurement. The specific surface areas for N$_2$ were calculated using the Brunauer-Emmet-Teller (BET) model in the range of $0.005 < P/P_0 < 0.1$. The pore size distributions of the MOFs were calculated from the adsorption-desorption isotherms by density functional theory (DFT) using the carbon slit-pore N$_2$-DFT model.

   The micropore volumes, micropore surface areas, and external surface areas for all samples were determined using conventional t-plot methods[S2] from N$_2$ adsorption data. For most of the MOFs, the values were selected over the 3-5 Å t range by fitting the data to the Harkins-Jura thickness equation. For HCl-UiO-67|$_{9/12}$, whose adsorption isotherm exhibits a mesoporous step (at 0.1-0.2 P/P$_o$), the t range values were selected by fitting the data to the Harkins-Jura thickness equation over a range that affords a physically sensible positive value for micropore volume while maintaining a correlation coefficient that is closest to 1. This is the process we used in a recent publication on hierarchical porous organic polymers[S3] and is recommended by Prof. A. W. Marczewski[S4] as well as the Micromeritics Instrument Corporation.[S5] For HCl-UiO-67|$_{9/12}$, the t range was thus selected to be 5.5-6.4 Å. We note that a similar process has also been applied by Li *et al* to characterize a series of mesoporous MOF nanoparticles.[S6]

Inductively coupled plasma optical emission spectroscopy (ICP-OES) analyses of As and Zr contents in the supernatants from the As-batch experiments were conducted on a Varian Vista-MDX model ICP-OES spectrometer (Varian Inc., Walnut

Creek, CA) located in the IMSERC facility of Northwestern University. This instrument is equipped with a CCD detector and an argon plasma to cover the 175-to-785 nm spectral range.

ICP-OES analyses of the acid-digested MOF samples (for Zr and S contents) were conducted on a Thermo Scientific™ iCAP™ 7600 ICP-OES spectrometer (Thermo Fisher Scientific Inc., Waltham, MA) located in the QBIC facility of Northwestern University. This instrument is equipped with a high performance solid-state CID86 chip detector, dual view (radial and axial) capability, and an argon plasma to cover the 166-to-847 nm spectral range. In a typical procedure, MOF samples (2-5 mg) were digested in a small amount (1 mL) of a mixture of 3:1 v/v conc. $HNO_3:H_2O_2$ (30 wt % in H_2O) by heating in a Biotage SPX microwave reactor (Biotage, Uppsala, Sweden, software version 2.3, build 6250) at 180 °C until the solution became clear (~30 min). This acidic solution was then diluted to 25 mL with ultrapure deionized H_2O and analyzed for Zr (339.198, 343.823, and 349.619 nm) content as compared to standard solutions.

For safety considerations, thiolated MOF samples (~ 2 mg) were digested using either one of the following two methods:

1. Unoptimized procedure, which was used for the earlier experiments in our study. MOF sample (~2 mg) was combined with 4 mL of dilute aqueous HF (prepared by diluting 3 mL of conc. HF (48%) to 30 mL with ultrapure deionized water in a 50 mL propylene centrifuge tube) in a 15 mL propylene centrifuge tube. The tube was capped and agitated at room temperature for 24 h on a Fisher Scientific standard vortex mixer (Fisher Scientific, Inc., Pittsburgh, PA) set at 4.5 speed dial number. After stopping the agitation, conc. HNO_3 (250 µL) was then added to the cloudy yellow sample, the tube was recapped and agitated for another 24 h to afford a less-cloudy, light-yellow, but still partially digested mixture. After stopping the agitation, another aliquot of conc. HNO_3 (500 µL) was added and the sample was recapped and then agitated for an additional 48 h, leading to no visible change. The agitation was then stopped and the centrifuge tube was transferred to a sonicator inside a well-ventilated hood. After several minutes of sonication, the sample was removed from the sonicator; conc. HCl (250 µL) was added; and the sample was capped and placed in a 60 ºC sand bath for 24 h. As the mixture was still visibly cloudy after this, more conc. HF (250 µL of a 48% solution) was added to the cooled down sample and the sample was recapped and heated at in a 70 ºC sand bath for 24 h. At this point, the sample has become colorless and not cloudy; however, it still contained a few visible white specks of solids. More conc. HF (100 µL of a 48% solution) was added to the cooled down sample and the sample was capped and heated in a 70 ºC sand bath for 24 h. The resulting clear solution (5.35 mL total volume of approximately 1:1:0.3:4.7 volumetric ratio of conc. HNO_3:conc. HF:conc. HCl:H_2O) was then transferred to a 50 mL propylene centrifuge tube in the hood and diluted to 50 mL with ultrapure deionized H_2O using a 5 mL Eppendorf Research mechanical pipettor. This acid-digested sample was then analyzed for Zr (339.198, 343.823, and 349.619 nm) and S (180.731 and 182.034 nm) contents as compared to standard solutions. *Caution: HF is very toxic and dangerous to handle without proper safety training. PPE must include Silvershield gloves and goggles. Acid digestions and subsequent dilutions should be carried out in a well-ventilated hood.*

2. Optimized procedure, which was used for the later experiments in our study. A digestion solution (5.35 mL total volume in 1:1:0.3:4.7 volumetric ratios of conc. HNO_3:conc. HF:conc. HCl:H_2O) was prepared by combining the reagents in the following order: conc. HNO_3 (750 µL), conc. HCl (250 µL), H_2O (3.6 mL), and conc. HF (750 µL). MOF sample (~2 mg) was combined with this mixture in a 15 mL propylene centrifuge tube, capped, and heated in a 70 ºC sand bath for 3 h. The resulting clear solution was then transferred to a 50 mL propylene centrifuge tube in the hood and diluted to 50 mL with ultrapure deionized H_2O using a 5 mL Eppendorf Research mechanical pipettor. This acid-digested sample was then analyzed for Zr (339.198, 343.823, and 349.619 nm) and S (180.731 and 182.034 nm) contents as compared to standard solutions.

Centrifugation was carried out in an Eppendorf Centrifuge 5804 R, Model AG 22331 (Eppendorf AG, Hamburg, Germany) equipped with an F34-6-68 rotor. Unless otherwise stated, all centrifugations were carried out at 5000 rpm (3214 g) for 10 minutes.

Thermogravimetric analysis (TGA) experiments were carried out on a Q500 thermogravimetric analyzer (TA Instruments Inc., New Castle, DE). Samples (~20 mg) were heated from room temperature to 600 ºC under an O_2-rich (30 vol % in nitrogen) gas flow (90 mL/min) at a heating rate of 5 ºC/min.

X-ray photoelectron spectroscopy (XPS) measurements were carried out at the Keck-II/NUANCE facility at Northwestern University (NU) on a ESCALAB 250 Xi instrument (Thermo Scientific, Waltham, MA) (Al Kα radiation, hv = 1486.6 eV) equipped with an electron flood gun. XPS data was analyzed using Thermo Scientific Avantage Data System software (v5.926) and all spectra were referenced to the adventitious C1s peak (284.5 eV). To have enough for sample for analysis, 5-6 MOF samples (~10 mg/MOF per sample) were subjected to the same As-adsorption batch experiment conditions (see section S2), combined, and vacuum-filtered over a Büchner funnel (Whatman filter paper Grade 2: 8um). The collected solids were subsequently rinsed over the Büchner funnel with water (2 × 20 mL), acetone (1 × 20 mL), and suction-dried for several hours. Prior to XPS measurements, the solid samples were thermally activated at 120 ºC under high vacuum to remove water from the pores.

Diffuse reflectance infrared Fourier-transformed spectroscopy (DRIFTS) experiments were carried out on a Nicolet Nexus 870 FTIR spectrometer (Thermo Scientific, Waltham, MA) equipped with an MCT detector. MOF samples (from the remaining sample prepared for XPS; see above) were first activated at 120-150 ºC under high vacuum for 24 h. These activated MOF samples (~ 3 wt %) were then combined with anhydrous KBr, grounded up thoroughly, and then loaded into the instrument as a powder. The spectra were collected at 1 cm^{-1} resolution over 64 scans under N_2 purge. A sample of powder KBr was utilized as the background. Spectra were converted to Kubelka-Munk units and normalized to the most prominent peak within the specified region.

Scanning electron microscopy (SEM) images were obtained at Northwestern University's EPIC/NUANCE facility on a SU8030 FE-SEM (Hitachi High Technologies America, Inc., Dallas, TX) microscope with an acceleration voltage of 10 kV. Prior to imaging, activated MOF samples were coated with either a film of Au/Pd or Os (~10-20 nm thickness) using either a Denton Desk III TSC Sputter Coater (Denton Vacuum, Moorestown, NJ) or a Filgen Osmium Coater Model OPC-60A (Filgen, Nagoya, Japan), respectively. Size measurements were obtained from sample populations of >70 particles, which were used to construct the standard normal distribution plots (mean ± 3 standard deviation units) and the histograms. Data are shown in Fig. S6.

Transmission electron microscopy (TEM) images and energy-dispersive X-ray spectroscopy (EDS) line scans were collected at Northwestern University's EPIC/NUANCE facility on a Hitachi HT-7700 Biological S/TEM (Hitachi High Technologies America, Inc., Dallas, TX) equipped with a Bruker EDS system with an accelerating voltage of 120 kV. MOF samples (1-2 mg) were sonicated in ethanol (~10 mL) until a well-dispersed solution was obtained. About 1-2 drops of the resulting solution was spotted on the TEM-grid and allowed to air-dry for a few minutes before TEM imaging.

ESI-MS spectra was collected in negative mode on an Agilent 6210 LC-TOF instrument located in the IMSERC facility of Northwestern University.

High-resolution water suppression ^{1}H NMR spectra of aqueous samples were obtained on an Agilent DD2 600 NMR spectrometer (Agilent Technologies, Santa Clara, CA) equipped with a triple resonance (HCN) cold probe w/ Z-gradient and a sensitivity of ^{1}H = 4300 and ^{13}C = 250. This high-resolution ^{1}H NMR instrument, located in the IMSERC facility of Northwestern University, was necessary to observe the BDC aromatic resonances at μM concentration under water-suppression mode.

S2. Synthesis of UiO analogues

AcOH-UiO-66|$_{11/12}$. In a 2 L Erlenmeyer flask, $ZrCl_4$ (1.86 g, 8 mmol) was dissolved by stirring in dimethylformamide (DMF, 500 mL) before being combined with glacial acetic acid (144 g, 137.3 mL, 2.4 mol). In a separate 1 L Erlenmeyer flask, terephthalic acid (1.33 g, 8 mmol) was dissolved completely in DMF (500 mL). This terephthalic acid solution was then added slowly to the $ZrCl_4$ solution and the combined mixture was stirred until homogenized. The resulting solution was partitioned evenly among fifty 8 dram vials. The vials were capped and placed in a 120 °C pre-heated oven for 24 h before being cooled to room temperature. The contents of the vials were combined and filtered over a fine-fritted funnel to afford the crude AcOH-UiO-66|$_{11/12}$ as a white powder, which was then rinsed with methanol (~ 50-80 mL). The collected materials were then immersed in methanol (~ 35 mL) and kept at 50-60 °C for an additional 24 h. After cooling, this mixture was filtered over a fine-fritted funnel and allowed to dry under continuous suction from the house vacuum until the white solid become non-sticky and can be collected and stored at room temperature. This solid (~1.5 g, ~70% yield based on $ZrCl_4$[S7]) was activated in portions at 150 °C under high vacuum before being used in As-uptake experiments.

We note that the synthesis protocol as described above is quite reliable and can give materials with a minimum of variation in missing linkers (AcOH-UiO-66|$_{(11.0 ± 0.2)/12}$) as determined by TGA, see Fig. S7), independent of the person who carried out the synthesis. As such, although our work was carried out with several different batches of materials from three different experimenters (H.G.T.N, C.-Y.C, or C.O.A) the results are consistent. For simplicity and clarity in the manuscript, we refer to all of these materials as AcOH-UiO-66|$_{11/12}$.

HCl-UiO-66|$_{9/12}$. In an 125 mL Erlenmeyer flask, $ZrCl_4$ (1.25 g, 5.4 mmol) was dissolved by sonication in a mixture of DMF (50 mL) and concentrated HCl (10 mL). In a separate 125 mL Erlenmeyer flask, terephthalic acid (1.23 g, 7.4 mmol) was dissolved by sonication in DMF (100 mL). This terephthalic acid solution was then added slowly to the $ZrCl_4$ solution and the combined mixture was stirred until homogenized. The resulting solution was then partitioned among ten 8 dram vials. The vials were capped and placed in a 80 °C pre-heated oven for 24 h before being cooled to room temperature. The contents of the vials were combined and filtered over a fine-fritted funnel to afford the crude HCl-UiO-66|$_{9/12}$ as a white powder, which was then rinsed with DMF (2 × 30 mL) and either ethanol or methanol (2 × 30 mL). The collected solid was left on the fritted glass funnel, which was connected to the house vacuum, covered with a glass crystallizing dish to allow for partial air flow through the funnel under reduced pressure, and allowed to be dried overnight in this fashion to

give a white solid (~1.4 g, >100% yield based on $ZrCl_4$[S7]) that is then stored at room temperature. Portions of this solid was activated at 150 °C under high vacuum as needed before being used in As-uptake experiments.

HCl-UiO-66|$_{x/12}$ derivatives. In a 250 mL Erlenmeyer flask, $ZrCl_4$ (1.5 g, 6.4 mmol) was dissolved by sonicating in a mixture of DMF (60 mL) and concentrated HCl (12 mL) for 1 h. This solution was then evenly distributed (15 mL per flask) into four separate 125 mL Erlenmeyer flasks. To each flask was then added solid terephthalic acid (801 mg, 3.22 mmol, for HCl-UiO-66 |$_{10.6/12}$; 534 mg, 2.22 mmol, for HCl-UiO-66|$_{y/12}$; 369 mg, 1.61 mmol, for HCl-UiO-66|$_{9/12}$; and 214 mg, 1.28 mmol, for HCl-UiO-66|$_{8.2/12}$, following by DMF (30 mL). The resulting mixtures were then homogenized via sonication.

Each of the aforementioned solutions was then evenly transferred to three 8 dram vials (~16 mL each). These vials were capped and placed in a 80 °C pre-heated oven overnight before being allowed to cool to room temperature. The vials of the same composition were combined and filtered over fine-fritted funnels to afford the crude MOFs as white powders, each of which was then rinsed with DMF (2 × 100 mL) and EtOH (2 × 100 mL). The collected solid was left on the fritted glass funnel, which was connected to the house vacuum, covered with a glass crystallizing dish to allow for partial air flow through the funnel under reduced pressure, and allowed to be dried overnight in this fashion to give white solids that are stored at room temperature. Portions of this solid was activated at 150 °C under high vacuum as needed before being used in As-uptake experiments.

Table S1. Preparative data for HCl-UiO-66|$_{x/12}$ ([$Zr_6O_4(OH)_4(L)_x$]).[a]

MOFs	Amount of organic linker used	MOF yield [S7] (mg)	Specific surface area (m²/g)
HCl-UiO-66|$_{10.6/12}$	801 mg (4.82 mmol)	~510	1400
[b]HCl-UiO-66|$_{y/12}$	534 mg (3.21 mmol)	~430	1600
[b]HCl-UiO-66|$_{9/12}$	369 mg (2.22 mmol)	~430	1650
HCl-UiO-66|$_{8.2/12}$	214 mg (1.29 mmol)	~350	1760

[a]See Fig. S4 for formula unit determination. [b]Yield, TGA, and As[V]-uptake data suggest no significant difference between these two batches.

AcOH-UiO-66-(SH)$_2$. In an 125 mL Erlenmeyer flask, $ZrCl_4$ (110.4 mg, 0.48 mmol) was dissolved by sonication in a mixture of DMF (30 mL) and acetic acid (8.2 mL, 8.5 g, 143 mol). In a separate 125 mL Erlenmeyer flask, 2,5-dimercaptoterephthalic acid (111.6 mg, 0.48 mmol) was dissolved in DMF (30 mL) by sonication. This solution was then added slowly to the $ZrCl_4$ solution and the combined mixture was stirred until homogenized. The resulting solution was paritioned among three 8 dram vials. These vials were capped and placed in a 120 °C pre-heated oven for 24 hours before being cooled to room temperature. The contents of the vials were combined and filtered over a fine-fritted funnel to afford the crude AcOH-UiO-66-(SH)$_2$ as a light-yellow powder, which was then resuspended in fresh DMF (~20 mL) in a capped 8 dram vial and placed in a 60 °C preheated oven for at least 3 h. After cooling to room temperature, this suspension was then filtered over a fine-fritted funnel; the collected solid was then resuspended in dichloromethane (DCM, ~20 mL) in a capped 8 dram vial and placed in a 60 °C pre-heated oven for at least 3 h. After cooling to room temperature, the suspension was then filtered over a fine-fritted funnel and the collected solid was rinsed with DCM (~ 20 mL). The collected solid was left on the fritted glass funnel, which was connected to the house vacuum, covered with a glass crystallizing dish to allow for partial air flow through the funnel under reduced pressure and allowed to be dried overnight in this fashion to give a light-yellow powder (~130 mg, ~79% yield based on $ZrCl_4$ [S7]) that is then stored at room temperature. Portions of this solid was activated at 100 °C under high vacuum as needed before being used in As-uptake experiments.

HCl-UiO-66-(SH)$_2$. In an 8 dram vial, $ZrCl_4$ (125 mg, 0.54 mmol) was dissolved by sonication in a mixture of DMF (5 mL) and HCl (1 mL). In a separate 8 dram vial, 2,5-dimercaptoterephthalic acid (170.5 mg, 0.74 mmol) was dissolved by sonication in DMF (10 mL). This solution was then added slowly to the $ZrCl_4$ solution and stirred until homogenized. The vial was capped and placed in a 80 °C pre-heated oven for 24 hours before being cooled to room temperature. The solid product was collected over a fine-fritted funnel, resuspended in fresh DMF (~20 mL) in a capped 8 dram vial, and finally placed in a 60 °C preheated oven for at least 3 h. After cooling to room temperature, this suspension was then filtered over a fine-fritted funnel; the collected solid was then resuspended in dichloromethane (~20 mL) in a capped 8 dram vial and placed in a preheated oven at 60 °C for at least 3 h. After cooling to room temperature, the suspension was then filtered over a fine-fritted funnel and the collected solid was rinsed with DCM (~ 20 mL). The collected solid was left on the fritted funnel, which was connected to the house vacuum, covered with a glass crystallizing dish to allow for partial air flow through the funnel under reduced pressure, and allowed to be dried overnight in this fashion to give a light-yellow powder

(~190 mg, 100% yield based on $ZrCl_4$ [S7]) that is then stored at room temperature. Portions of this solid was activated at 100 °C under high vacuum as needed before being used in As-uptake experiments.

HCl-UiO-66-(OH)$_2$. In an 8 dram vial, $ZrCl_4$ (125 mg, 0.54 mmol) was dissolved by sonication in a mixture of DMF (5 mL) and HCl (1 mL). In a separate 8 dram vial, 2,5-dihydroxyterephthalic acid (146.6 mg, 0.74 mmol) was dissolved by sonication in DMF (10 mL). This solution was then added slowly to the $ZrCl_4$ solution and stirred until homogenized. The vial was capped and placed in a 80 °C pre-heated oven for 24 hours before being cooled to room temperature. The solid product was collected via centrifugation and resuspended in fresh DMF (~20 mL) in a capped 8 dram vial, and finally placed in a 60 °C preheated oven for at least 3 h. After cooling to room temperature, the solid was separated from the suspension using centrifugation and then resuspended in dichloromethane (~20 mL) in a capped 8 dram vial. This suspension was placed in a preheated oven at 60 °C for at least 3 h. The collected solid was then dried in a vacuum oven overnight to give a light-yellow powder (~183 mg, 100% yield based on $ZrCl_4$ [S7]) that is then stored at room temperature. Portions of this solid was activated at 100 °C under high vacuum as needed before being used in As-uptake experiments.

HCl-UiO-67|$_{9/12}$. In a 125 mL Erlenmeyer flask, $ZrCl_4$ (335 mg, 1.44 mmol) was dissolved by sonicating in DMF (25 mL) and HCl (2.5 mL). In a separate 125 mL Erlenmeyer flask, biphenyl-4,4′-dicarboxylic acid (450 mg, 1.86 mmol) was partially dissolved by sonicating in DMF (25 mL). This dicarboxylic acid solution was then added slowly to the $ZrCl_4$ solution and stirred until homogenized. The resulting mixture was then partitioned among five 8 dram vials. The vials were capped and placed in an 80 °C pre-heated oven for 24 h before being cooled to room temperature. The contents of the vials were combined and the tan-white powder was collected over a fine-fritted funnel and rinsed with DMF (2 × 30 mL) and ethanol or methanol (2 × 30 mL). The collected solid was left on the fritted glass funnel, which was connected to the house vacuum, covered with a glass crystallizing dish to allow for patial air flow through the funnel under reduced pressure, and allowed to be dried overnight in this fashion to give a white solid (~777 mg, >100% yield based on $ZrCl_4$ [S7]) that is then stored at room temperature. Portions of this solid was activated at 150 °C under high vacuum as needed before being used in As-uptake experiments.

S3. Arsenic batch-adsorption experiments

Stock solutions (1 L) with predetermined concentrations of As^{III} (As_2O_3) and As^V ($NaHAsO_4•7H_2O$) were prepared prior to adsorption experiments. Typically, the solid reagent was dissolved by sonication in ultrapure deionized H_2O to give a clear solution. The pH of the resulting solution was measured and adjusted to pH ~7 for As^V and pH ~5 for As^{III} using HCl and NaOH when necessary. The pH values of these solutions remain constant for months after preparation and during experimentations. The As concentrations were verified with ICP-OES at the beginning of each batch-adsorption experiment (t = 0).

Arsenic batch-adsorption experiments were carried out in 50 mL VWR polypropylene centrifuge tubes. In a typical experiment, activated MOF (~10 mg) was added as a solid to a centrifuge tube containing a 50 ppm solution (30 mL) of As^{III} (As_2O_3) or As^V ($NaHAsO_4•7H_2O$). The tubes were capped and gently agitated using a Barnstead Thermolyne Labquake Shaker Rotisserie Model T400110 (Barnstead International, Dubuque, IA). At specified time intervals, the tubes were centrifuged at 3214 g for either 1 or 10 min (see below) before an aliquot (~3.5 mL) of the supernatant was removed using a disposable syringe and passed through a 0.2 μm PTFE syringe filter (VWR International, North American Cat. No. 28145-495) into a 15 mL VWR polypropylene centrifuge tube. The collected liquid samples were then directly analyzed for Zr (327.307, 343.823, and 349.619 nm) and As (188.98 and 228.812 nm) content as compared to standard solutions. The amount of arsenic uptake at each time point t is calculated as the difference between the initial As amount and the amount found in the supernatant solution at t.

For the uptake profiles shown in Figs. S9-11, as well as Figs. 3 and 6 in the manuscript, each tube was agitated until a specified amount of time (i.e., 0.5, 3, 6, 24 hours), at which the tubes were centrifuged for 10 min before sample aliquots were taken.

For the comparative kinetic studies (i.e., data shown in Figs. S12-14), where several data points were taken during the first 30 minutes of contact time, each tube was agitated for 4 minutes and then centrifuged for 1 minute before sample aliquots were taken.

We note that there is no leaching of Zr^{IV} ions from the MOF samples under all of the aforementioned experimental conditions. In fact, exposing samples of AcOH-UiO-66|$_{11/12}$ (10 mg) to a range of solutions with different As^V concentrations (30 mL of 100-1000 ppm As^V) does not lead to detectable zirconium ions in any of the solutions after 24 h. (Under these conditions, 1 ppm Zr^{IV} in the supernatant is equivalent to 1% MOF degradation).

Stability of MOFs under the batch-adsorption conditions. Samples of HCl-UiO-66|$_{9/12}$, AsOH-UiO-66|$_{11/12}$, and HCl-UiO-67|$_{9/12}$ were exposed to a 50 ppm solution (30 mL) of As^V ($NaHAsO_4•7H_2O$) for 24 h, isolated by centrifugation, air-

dried, and examined with PXRD. The PXRD pattern of each MOF sample after As^V treatment (Figs. S1,S3) is identical to that of the starting materials, suggesting that the crystallinity of the samples are maintained. Analysis of the remaining As-containing supernatant by ICP-OES does not show any Zr^{IV} ions from the MOF samples.

While we did not observe the loss of sample crystallinity via PXRD and loss of Zr^{IV} ions during As^V batch-adsorption experiments, it is possible that the Zr-containing degradation products, if any, could be amorphous and precipitate out of the solution. A related scenario is when As^V species would bind around nodes in a MOF unit cell (see Fig. S21 below), sterically displace the adjacent BDC linkers, and oligomerize more As^V ions around the node, as during one of secondary binding processes discussed in the manuscript. Such a linker-displacement mechanism[S8] would allow for more As^V binding at a node beyond the available defect sites. To address such possibility of ligand loss, we carried out ICP-OES, ESI-MS, and water suppression ^1H NMR analyses of the supernatant solutions that were separated from three UiO-66 samples (HCl-UiO-66|$_{9/12}$, AcOH-UiO-66|$_{11/12}$, and HCl-UiO-66(SH)$_2$|$_{10.5/12}$) after a batch treatment with arsenates (30 mL of 50 ppm As^V, 24 h exposure). Consistent with the batch-adsorption experiments described above, Zr-leaching was not observed by ICP-OES for all three As^V-treated samples. However, the ESI-MS spectrum of the aqueous supernatant remained after As^V-treatment of HCl-UiO-66|$_{9/12}$ sample, which is the most likely to lose ligands due to its high missing-linker density, revealed the presence of the BDC linker. These data are consistent with the possibility described at the beginning of this paragraph where linker replacement occurs without loss of nodes. Unfortunately, TGA analysis of the As-treated MOF could not be conducted due to safety reasons and the potential overlap of the arsenic oxide volatiles at 425 °C,[S9] a temperature that is too close to the loss of the H_2BDC and $H_2BDC(SH)_2$ linkers.

Additional ICP-OES sulfur analysis of the batch-experiment supernatant for HCl-UiO-66(SH)$_2$|$_{10.5/12}$, revealed that only 0.8 ± 0.2 % of the MOF linkers was leached into solution after the 24 h batch-adsorption experiment, suggesting that degradation is minimal for this sample. Unfortunately, our attempts to use water-suppression ^1H NMR spectroscopy to directly quantify the amount of BDC linkers in the supernatants isolated from the batch-adsorption experiment for AcOH-UiO-66|$_{11/12}$ and HCl-UiO-66|$_{9/12}$ were not successful due to the low solubility of H_2BDC (1.7 mg/100 mL H_2O at 20 °C), which prevents the construction of a calibration curve. Attempts to remedy this (i.e., adding DMSO-d_6, dilution, adjusting of the solution pH) all led to the irregular integration values against maleic acid, sodium acetate, and MeOH internal standards, possibly due to the undesired complexation of the remaining arsenates with the linkers. However, qualitative comparison of the water-suppressed ^1H NMR spectra of the three supernatants HCl-UiO-66(SH)$_2$|$_{10.5/12}$ does confirm that the amount of leached-out linkers in the supernatant was highest for the more-defective HCl-UiO-66|$_{9/12}$, and lowest for HCl-UiO-66(SH)$_2$|$_{10.5/12}$.

Although all of our data to date do not conclusively address the question of MOF stability, it is worthwhile to note that the As concentrations that we explored for the uptake experiments herein are much higher than those exists in nature (1 ppb - 3 ppm),[S10] which could accelerate secondary linker-displacement mechanism such as those mentioned in the manuscript. With this caveat, our observation of linker loss under these high exposure concentrations is not inconsistent with the linker-displacement binding mechanisms that have been proposed for arsenates[S8] and phosphates[S11] binding to MOFs with UiO-type nodes. While none of these other studies quantify both Zr^{IV} ion and linker loss, Lin and coworkers[S11] demonstrated the complete phosphate-replacement of the BDC linkers in UiO-66 at high phosphate exposures (50 mg MOF, 10 mL of 0.25 M H_3PO_4, corresponding to a 78.2 P:Zr$_6$ ratio).

**S4. Characterization data for UiO samples**
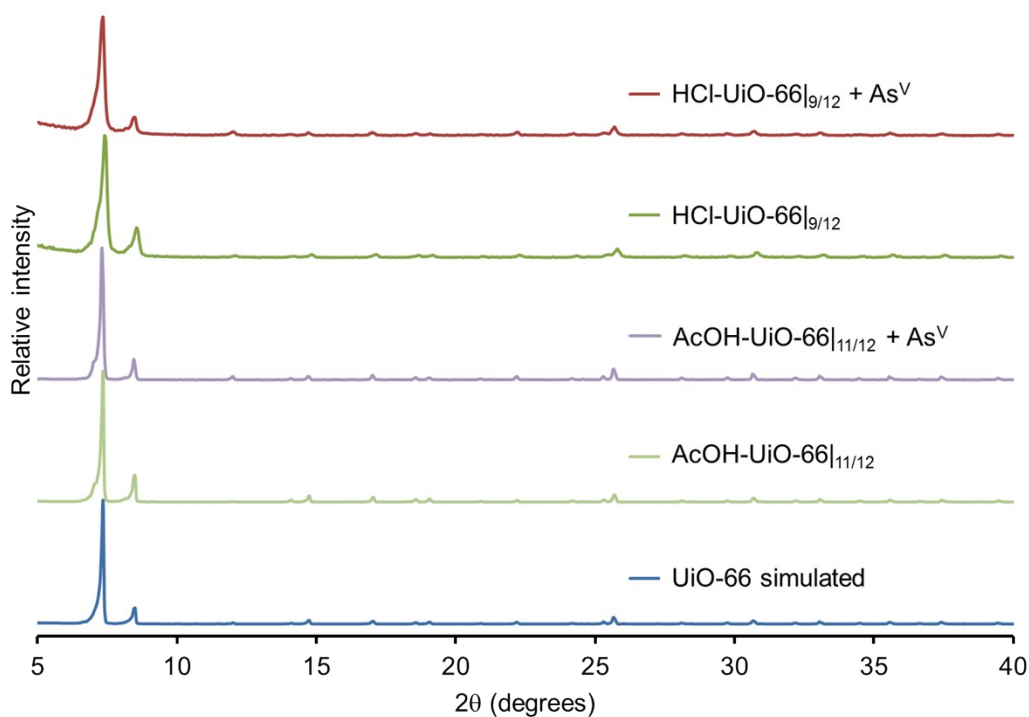
Fig. S1.   PXRD patterns of as-prepared UiO-66 analogues before and after exposure to aqueous As^V solutions for at least 24 h. The simulated PXRD pattern for UiO-66 is also included for comparison. As suggested by this data, the UiO-MOF samples are still crystalline after long exposures to aqueous As^V solution.
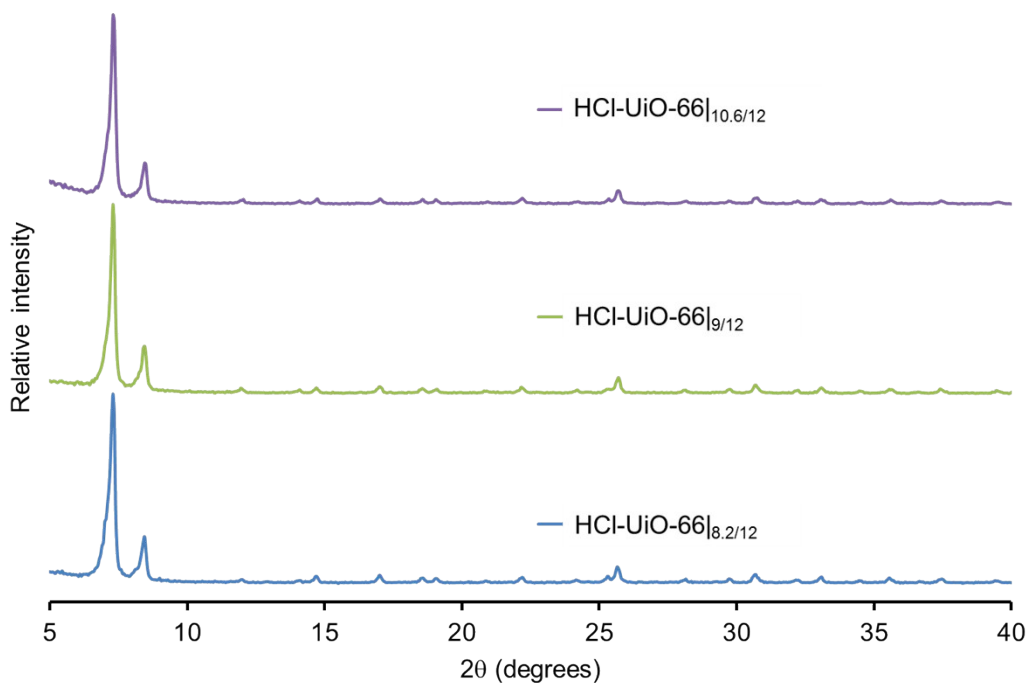
**Fig. S2**.   PXRD patterns of as-prepared HCl-UiO-66|$_{x/12}$ derivatives.
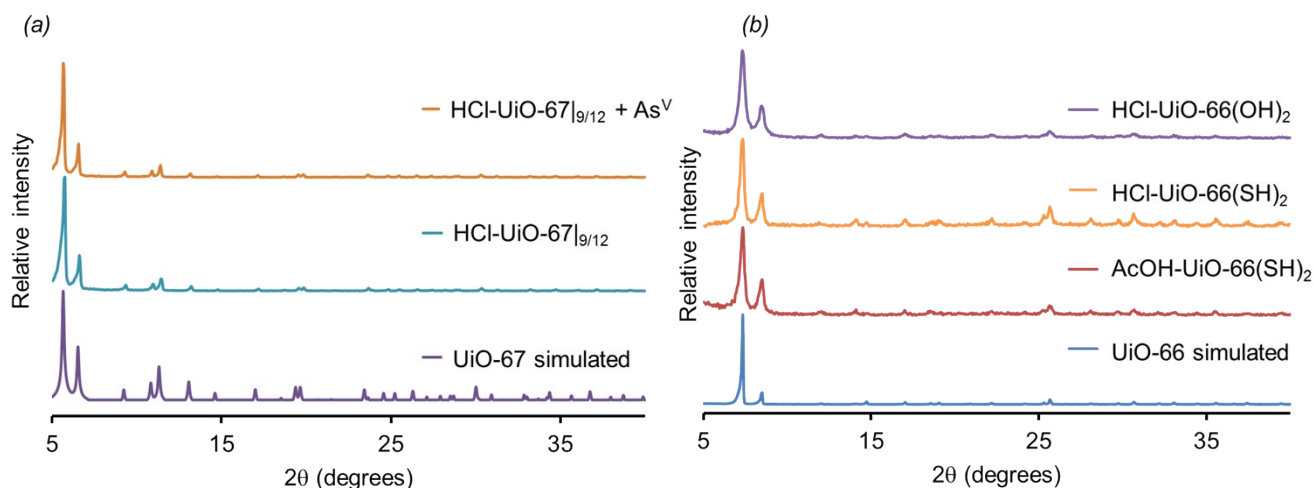
Fig. S3.   (a) PXRD patterns of as-prepared HCl-UiO-67|$_{9/12}$ before and after exposure to solutions of As^V. Good PXRD data can be obtained for As^V-exposed HCl-UiO-67|$_{9/12}$ upon solvent exchange to acetone from water and subsequent thermal activation.[S12]   Although UiO-67 has been reported to be unstable in water or mild acid/base aqueous solutions,[S13] this data suggest that our HCl-UiO-67|$_{9/12}$ retains crystallinity under our testing conditions. The simulated PXRD pattern for UiO-67 is also included for comparison. (b) PXRD patterns of as-prepared functionalized UiO-66 analogues (AcOH-UiO-66(SH)$_2$, HCl-UiO-66(SH)$_2$ and HCl-UiO-66(OH)$_2$). The simulated PXRD pattern for UiO-66 is also included for comparison.
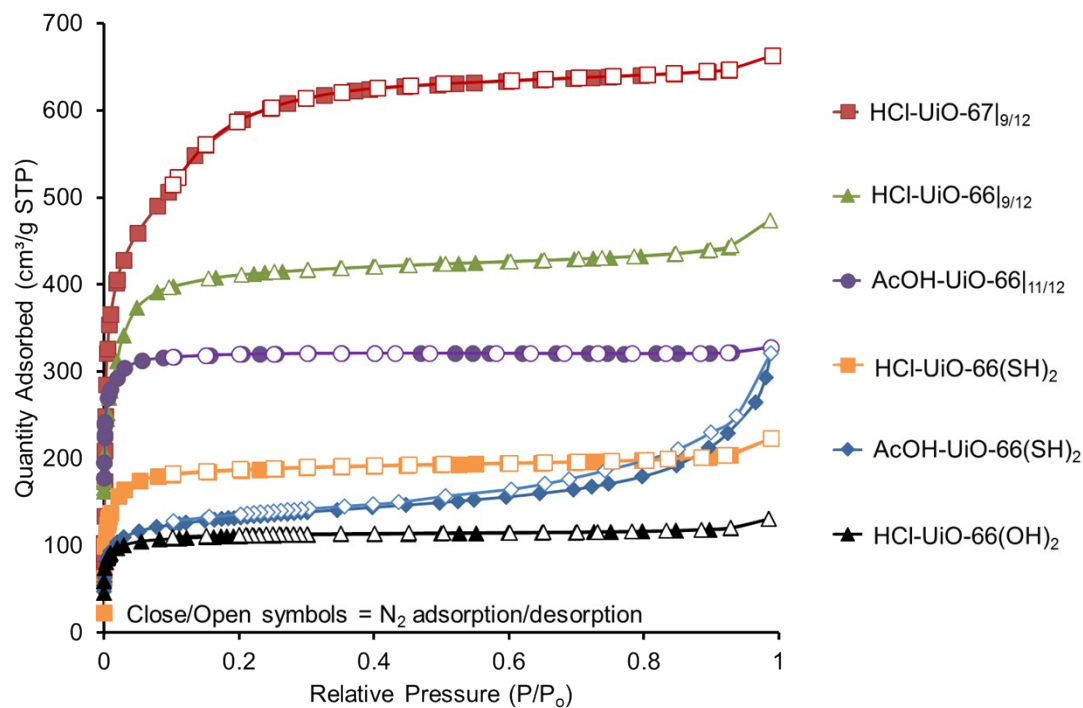
Fig. S4.   N$_2$ isotherms for the UiO-66 analogues used in this study.
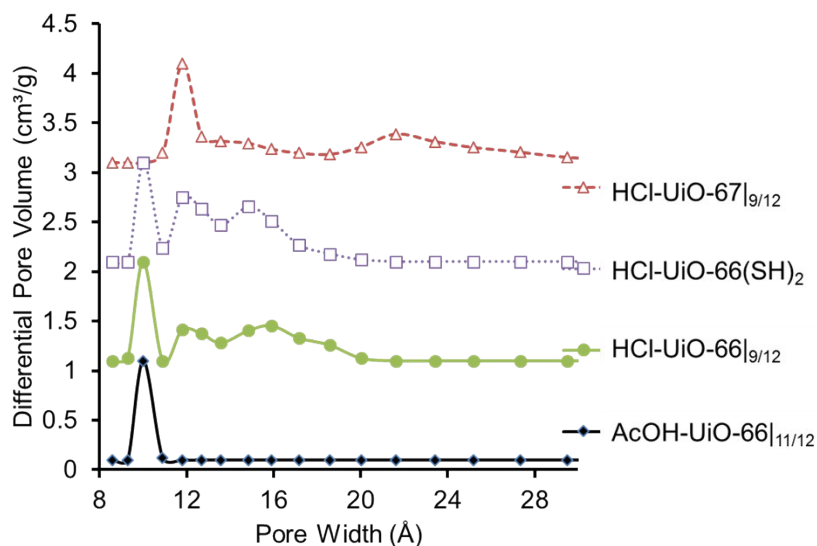
Fig. S5.   Relative pore size-distribution profiles for the UiO-66 analogues grown with different acid modulators. Data were collected on a Tristar II 3020 instrument, which does not allow for accurate evaluate of pore sizes < 8 Å. In comparison to the nearly defect-free AcOH-UiO-66|$_{11/12}$ sample, HCl-UiO-66|$_{x/12}$ derivatives, which have many missing-linker sites, clearly have additional larger pores (12-16 Å) that can increase accessibilityto the internal binding sites. The appearance of these additional pores as a result of missing linker formation is in aggrement with the analysis reported by Katz *et al* for UiO-66 samples with up to four missing linkers.[S14] We note that while the main micropore peak for AcOH-UiO-66|$_{11/12}$ (~10 Å) appears to be ~1-1.5 Å greater than the reported value for UiO-66,[S14-16] this is an artificial limitation of the instrumentation and does not affect the conclusion of our work. Consistent with this analysis, HCl-UiO-67, which has a larger diphenyldicarboxylate linker than HCl-UiO-66, expectedly has a larger main pore (12 Å) which is consistent with the reported value (11.5 Å).[S14]

Table S2.   Pore and surface properties of MOFs.

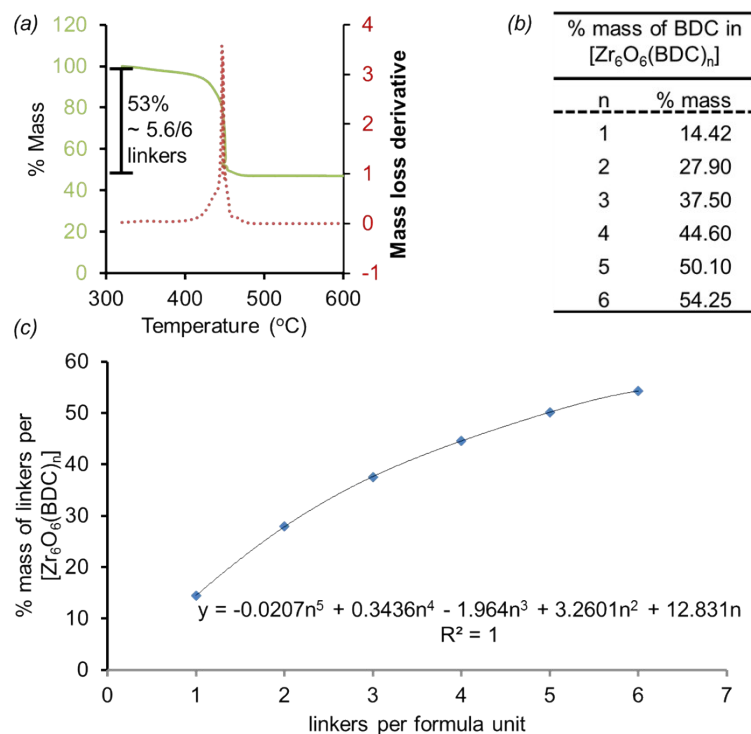| MOF	Specific surface area (m²·g⁻¹)	Total pore volume (cm³·g⁻¹)	Micropore volume (cm³·g⁻¹)	Micropore surface area (m²·g⁻¹)	External surface area (m²·g⁻¹)
AcOH-UiO-66|$_{11/12}$	1150	0.45	0.40	1080	70
HCl-UiO-66|$_{8.2/12}$	1760	0.72	0.56	1470	290
HCl-UiO-66|$_{9/12}$	1650	0.68	0.53	1390	260
HCl-UiO-66|$_{10.6/12}$	1480	0.64	0.47	1230	250
HCl-UiO-67|$_{9/12}$	2200	1.00	0.90	2100	100
AcOH-UiO-66(SH)$_2$	500	0.21	0.13	330	170
HCl-UiO-66(SH)$_2$	750	0.32	0.24	640	110
HCl-UiO-66(OH)$_2$	440	0.18	0.15	390	50
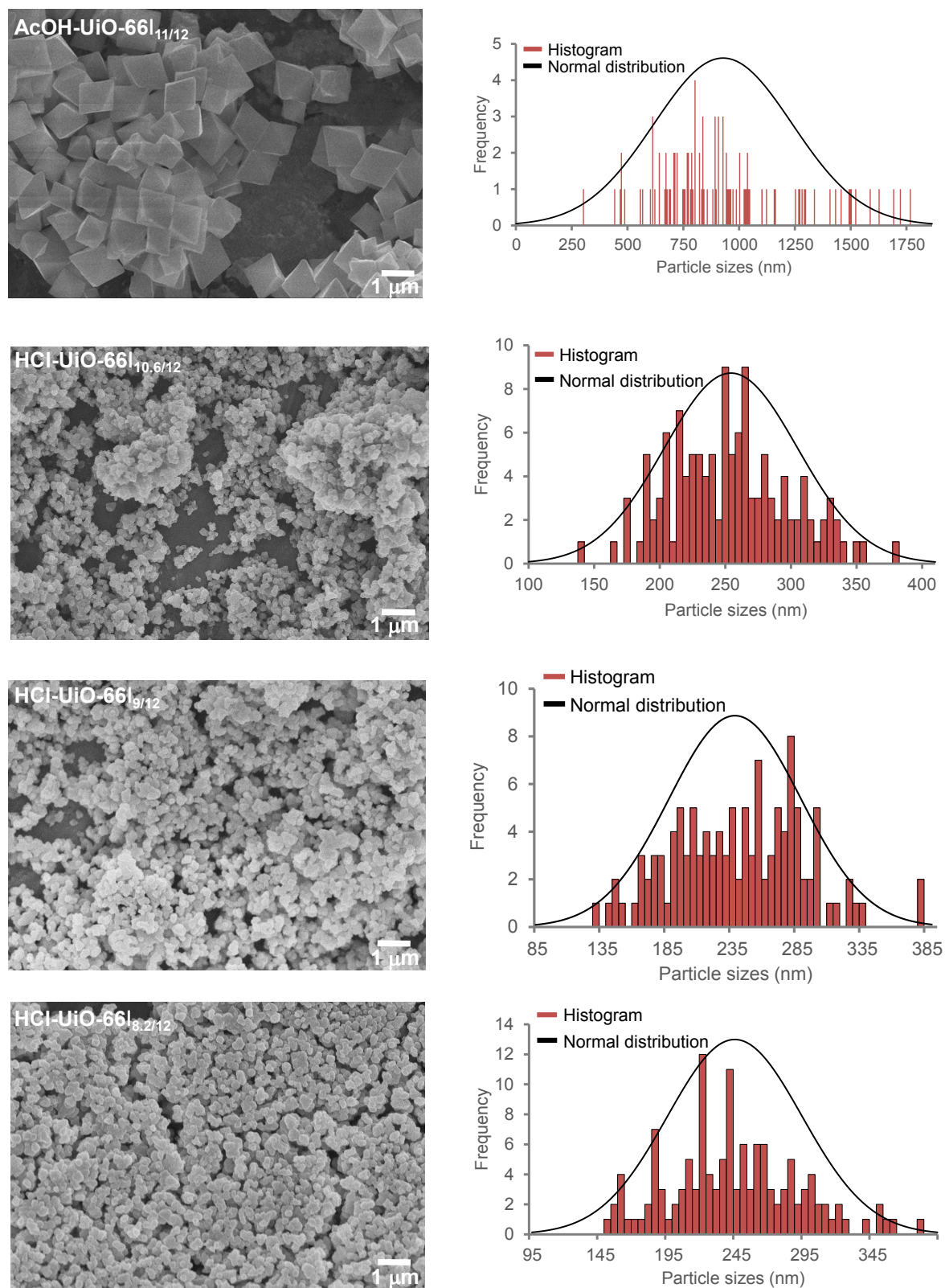
Fig. S6a. Left panels: SEM images of AcOH-UiO66|$_{11/12}$ and HCl-UiO66|$_{x/12}$ MOFs. Right panels: The corresponding SEM-derived particle-size-distribution profile for the MOF samples; each profile was constructed based on measurements of >70 particles.
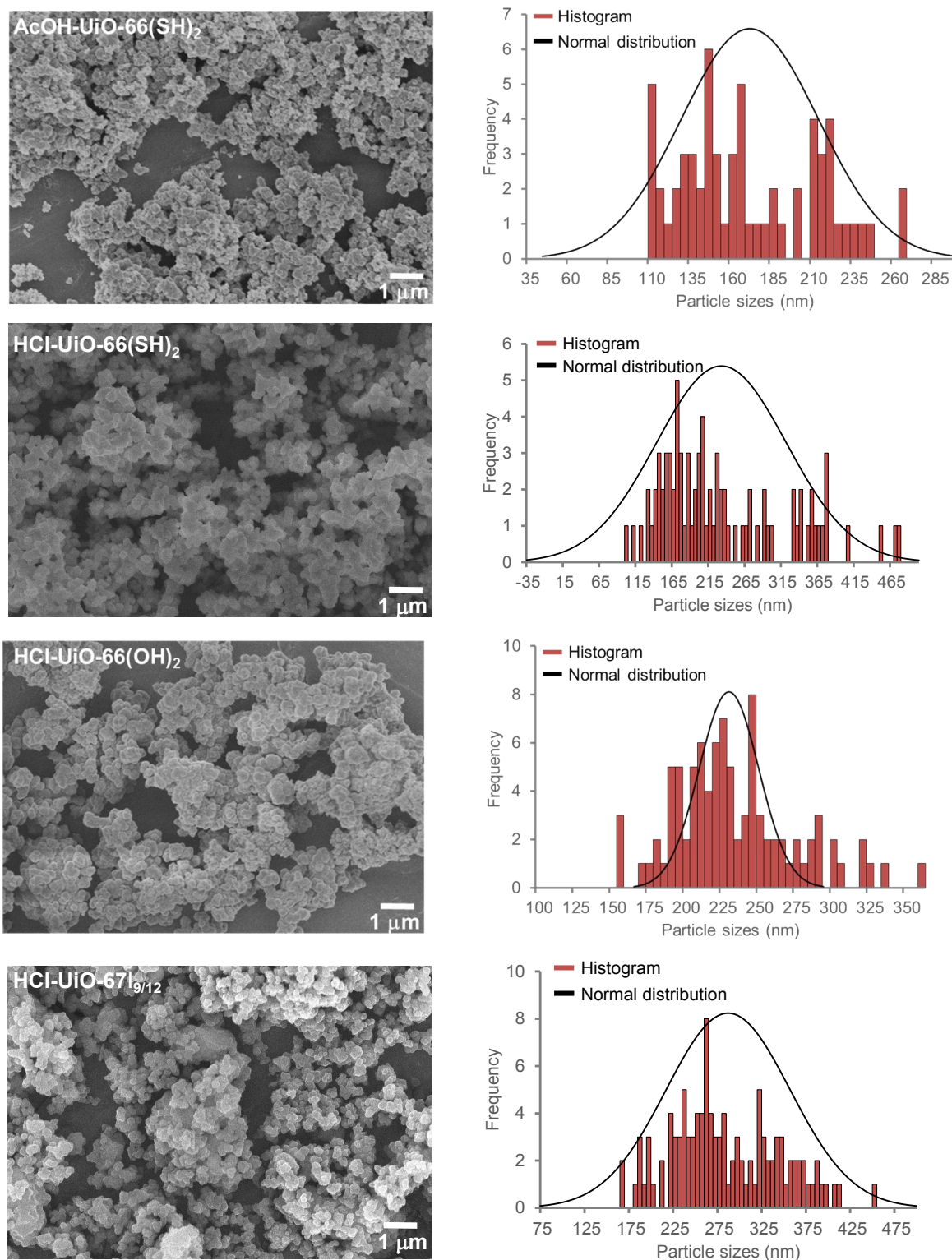
Fig. S6b. Left panels: SEM images of AcOH-UiO-66-(SH)$_2$, HCl-UiO-66-(SH)$_2$, HCl-UiO-66-(OH)$_2$, and HCl-UiO-67|$_{9/12}$ MOFs. Right panels: The corresponding SEM-derived particle-size-distribution profile for each of the MOF samples; each profile was constructed based on measurements of >70 particles.

S5. Determination of missing linker defects in UiO analogues

(b) % mass of BDC in $[Zr_6O_6(BDC)_n]$	
n	% mass
1	14.42
2	27.90
3	37.50
4	44.60
5	50.10
6	54.25

(c)

$$y = -0.0207n^5 + 0.3436n^4 - 1.964n^3 + 3.2601n^2 + 12.831n$$
$$R^2 = 1$$

Fig. S7.   The calculation of number of missing linkers for MOFs with $[Zr_6O_4(OH)_4(BDC)_n]$ compositions based on TGA profiles. (a) A representative TGA profile (green) for one AcOH-UiO-66$|_{11/12}$ sample and the first derivative (red-dotted line) of this profile, used to identify the point of complete linker degradation; where the only materials left is presumably ZrO_2. The total mass loss due to the organic linker is calculated from the mass at 320 °C, at which point the MOF is fully activated to the dehydoxylated $[Zr_6O_6(BDC)_n]$ compositions,[S17, 18] to the point of complete linker degradation. (b) A table showing theoretical % mass loss as a function of n. These % mass losses are the corrected values for the formation of ZrO_2 (instead of ZrO when derived directly from the $[Zr_6O_6(BDC)_n]$ formula (*ca.* 5.9% mass difference)). (c) Plot of the theoretical % mass vs n as best-fitted ($R^2 = 1$) to a polynomial equation. With this equation, convenient estimates of the amounts of missing linkers can be qualitative obtained from experimental data with a precision of 11.0 ± 0.1 linkers per node, as determined from six repetitive measurements of the same batch of AcOH-UiO-66$|_{11/12}$. Attempts to corroborate this data using the weight percent of Zr in a relatively small (4.5 mg, digestion of larger samples can lead to safety hazards in our equipments) sample of activated AcOH-UiO-66$|_{11/12}$ gave us 32 wt % Zr which is 1 wt % off from the theoretical 33 wt % Zr for $[Zr_6O_4(OH)_4(BDC)_{5.5}(AcO^-)_{0.5}]$. While this value is in aggreement with our formula unit, the error in the ICP-OES method, due to the reliance on accurate mass measurement of a very hygroscopic solid under ambient conditions and/or complete MOF digestion, prevents us from determining the accurate number of missing linkers. In contrast, the use of TGA allows us to use a much larger sample (20-30 mg) where adsorbed water and solvents can be completely removed prior to the decomposition temperature, and bypass these sources of error. As such, we estimated our amounts of missing linker present in the MOF using linker mass loss from 320-500 °C. It is important to note that the specific surface areas of these MOF samples correlate very well with the number of missing linkers (i.e., the more linkers missing in the sample, the higher the surface area) and these results are in aggreement with previously reported observations.[S14, 17, 19]
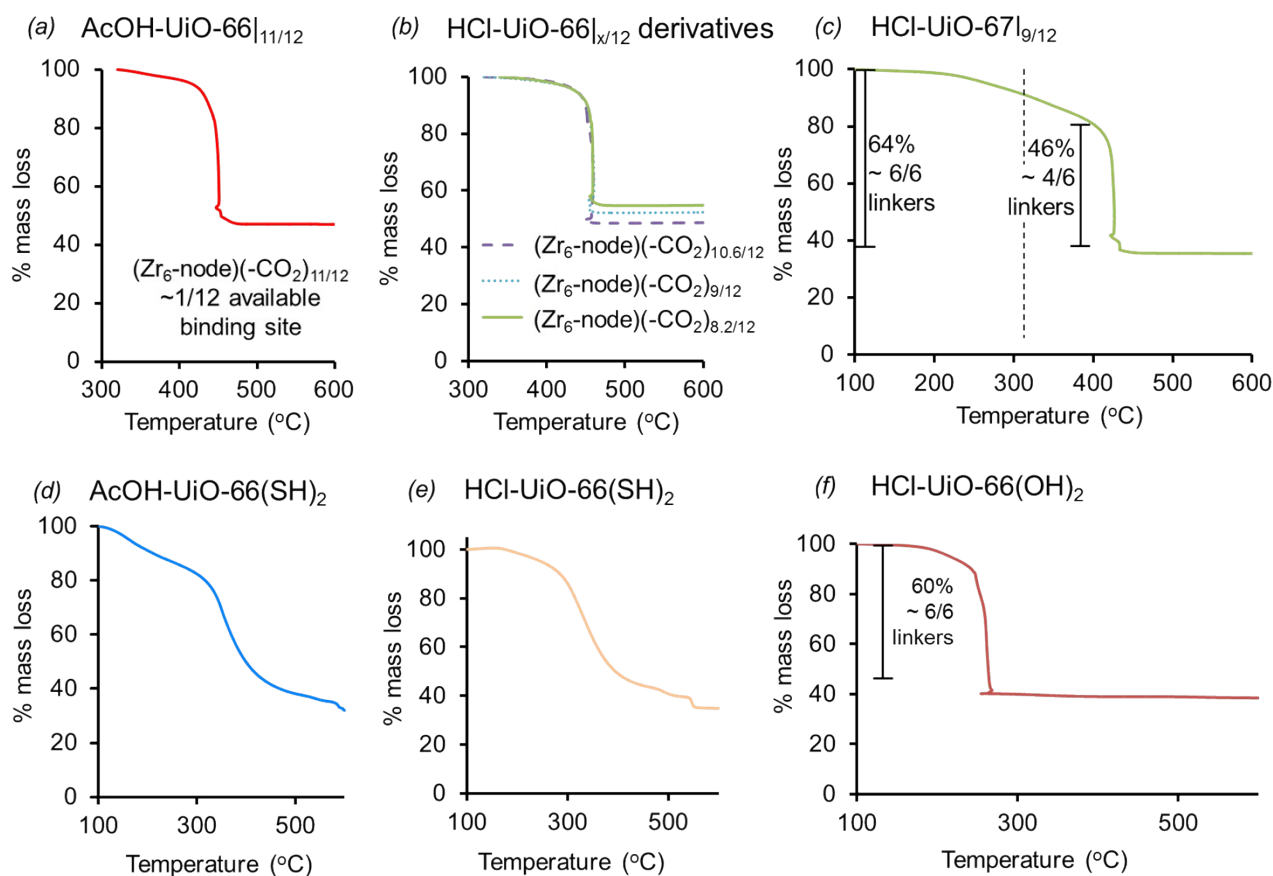
Fig. S8. (a-c) TGA profiles of AcOH-UiO-66|$_{11/12}$ (a), HCl-UiO-66|$_{x/12}$ derivatives (b), and HCl-UiO-67|$_{9/12}$ (c). For the TGA profile of HCl-UiO-67|$_{9/12}$, we set the linker-mass-loss point as 320 °C (dotted line) to be consistent with those for the UiO-66 samples, which were carried out under the sa me oxygen-enriched atmosphere. While our TGA profile for this sample does not exhibits a clear organic-mass-loss step at ~500 °C as reported by Katz *et al.*,[S14] their experiments were carried out in a N_2 atmosphere where complete oxidation of the organic is difficult. (d-f) TGA profiles for AcOH-UiO-66(SH)$_2$ (d), HCl-UiO-66(SH)$_2$ (e), and HCl-UiO-66(OH)$_2$ (f). As the TGA profiles of both thiolated MOFs show a gradual degradation with indistinct steps, predicting the amount of linkers present in them using TGA, as discussed in the caption of Fig. S7, is difficult. As such, we relied on the ICP-OES determination of the Zr:S ratio, which does not rely on weight % measurements and should accurately reflect the node/linker ratio in each sample. For both AcOH-UiO-66(SH)$_2$ and HCl-UiO-66(SH)$_2$, the Zr:S ratio were 1:(1.78 ± 0.03), suggesting that both samples have similar number of missing-linker defects (~10.5/12 carboxylates per node; a non-defective sample would yield a 1:2 Zr:S ratio, corresponding to 12/12 carboxylates per node). We note in passing that this analysis results in a higher number of missing-linker defects for our AcOH-UiO-66(SH)$_2$ sample than that reported by Yee *et al*,[S16] for a materials synthesized at 3 × [Zr] and with a smaller amount of AcOH modulator. Yee *et al* also estimmnated node/linker ratio using a combination of TGA under nitrogen flow[S20] and CHN combustion analysis, techniques that require estimates of trapped solvent or water.

S6. Data for the arsenic batch-adsorption analysis
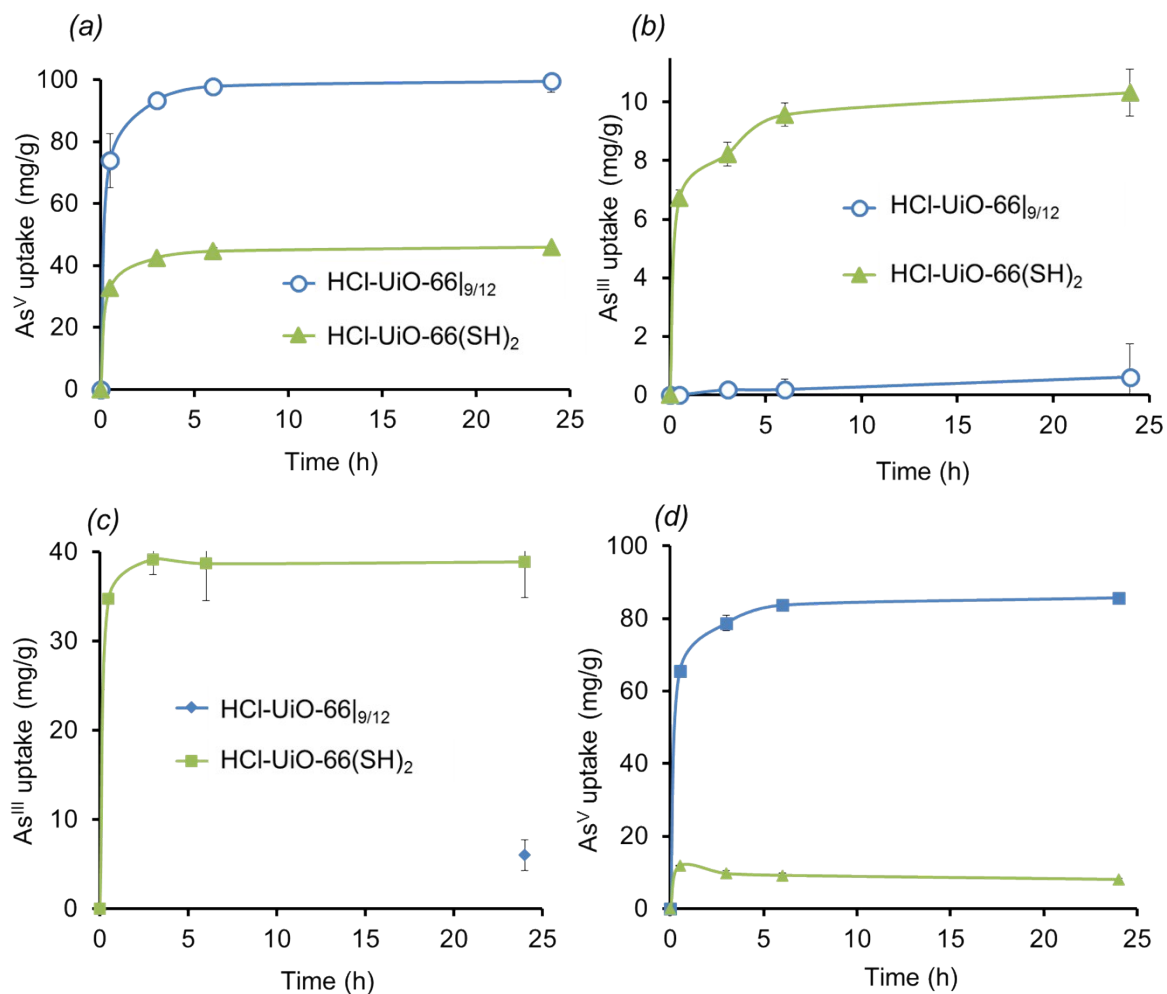


Fig. S9.   (a,b) These panels are reproductions of Fig. 6b-c in the main text for convience of the readers. Time-dependent arsenic-uptake profiles for HCl-UiO-66|$_{9/12}$ and HCl-UiO-66(SH)$_2$ samples in sequential exposure to As^V first (a), then As^{III} (b). (c,d) Time-dependent arsenic-uptake profiles for HCl-UiO-66|$_{9/12}$ and HCl-UiO-66(SH)$_2$ samples in the reverse exposure order (As^{III} first (c), then As^V (d)). Experimental conditions for all experiments: batch exposure of a sample of MOF (10 mg) to the appropriate As-containing solution (30 mL; 50 ppm initial concentration, pH ~ 7 for As^V stock solution and pH ~5 for As^{III} stock solution[S21]).
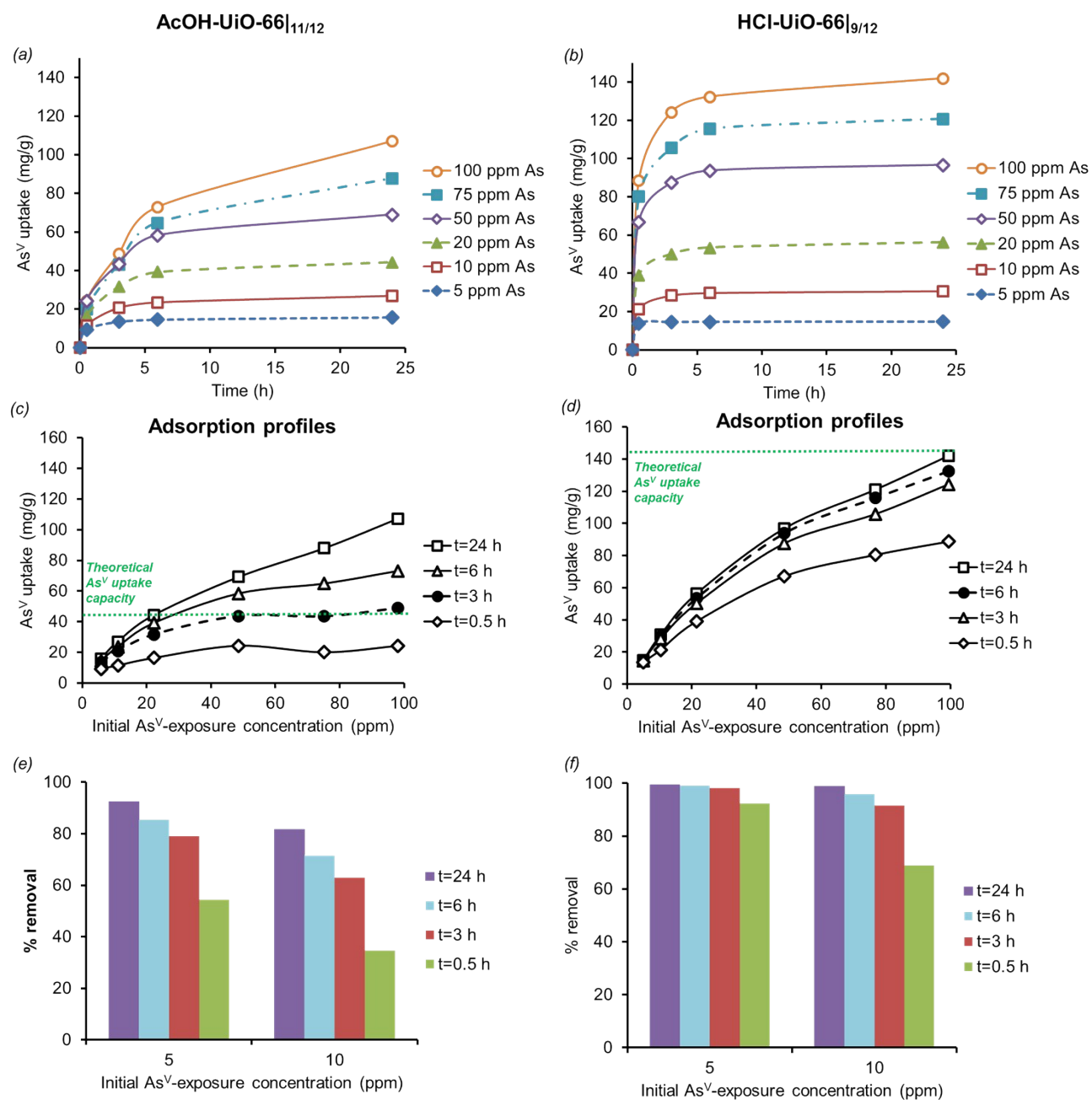
Fig. S10. (a,b) The time-dependent uptake profiles at different concentrations for AcOH-UiO-66|$_{11/12}$ (a) and HCl-UiO-66|$_{9/12}$ (b). (c,d) As^V-adsorption profiles (in mg/g) for AcOH-UiO-66|$_{11/12}$ (c) and HCl-UiO-66|$_{9/12}$ (d). The green dashed line across the y axis represents the theoretical As^V-uptake capacity *based* on the amount of missing linkers present in the sample. (e,f) % removal of As^{V}oxyanions from 30 mL solutions at different times and at low initial As^V-exposure concentrations for AcOH-UiO-66|$_{11/12}$ (e) and HCl-UiO-66|$_{9/12}$ (f). Experimental conditions: batch exposure of a sample of MOF (10 mg) to the appropriate As^V-containing solution (30 mL; 50 ppm initial concentration).

Interestingly, AcOH-UiO-66|$_{11/12}$ and HCl-UiO-66|$_{9/12}$ behaves very differently over time with respect to the concentration of the As^V in solution. When the initial As^V-exposure concentrations ≤ 20 ppm, the time-dependent As^V-uptake profile for AcOH-UiO-66|$_{11/12}$ plateaus after 6 h (Fig. S10a). The 6 h plateau behavior for the 20 ppm exposure is notable because it signifies that the AcOH-UiO-66|$_{11/12}$ has reached its theoretical capacity based on missing linker sites (Fig. S10c). However, at concentrations > 20 ppm, the uptake profiles continues to increase after 6 h (Fig. S10a), albeit at a much slower rate than the initial fast uptake. We attribute this behavior to the presence of a secondary uptake mechanism beyond the saturation of the estimated available binding sites due to missing linkers. As mentioned in the main text, such secondary uptake mechanisms could include the formation of As oligomers[S22] on the nodes (see Fig. S22a for an illustration) and/or linker

displacement.[S8] These secondary uptake mechanisms are not significant in our time-dependent As^V-uptake experiments for HCl-UiO-66|$_{9/12}$ (Fig. S10b) because these missing linker sites have not been fully saturated even at 100 ppm initial As^V-exposure concentration and after 24 h (Fig. S10d).
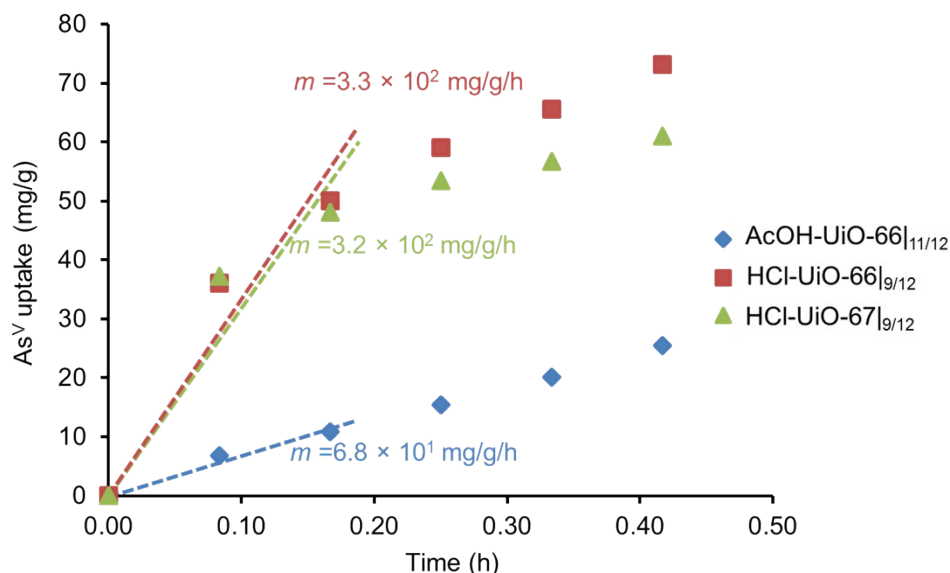
Fig. S11. Initial As^V-uptake profiles for MOF samples that have been exposed to a 50 ppm initial concentration of As^V. Given the long sampling time of the data-taking processes, only the first 3 data points could be used in the fits to get initial rate data before the pseudo-first-order assumption becomes invalid for HCl-UiO-66|$_{9/12}$ and HCl-UiO-67|$_{9/12}$ (over 25% of the As^V in solution has been uptaken). These data clearly shows that the rates for HCl-UiO-66|$_{9/12}$ and HCl-UiO-67|$_{9/12}$ are several times faster than AcOH-UiO-66|$_{11/12}$. We attribute this difference to two different effects: 1) The large particle size differences between AcOH-UiO-66|$_{11/12}$ and the HCl-capped MOFs: HCl-UiO-66|$_{9/12}$ and HCl-UiO-67|$_{9/12}$ have particles that are 4 times smaller in comparison to those for AcOH-UiO-66|$_{11/12}$. 2) The fast diffusion into the first few layers of the MOF particles as a result of larger amounts of defects (hence larger pore sizes) in the HCl-prepared MOFs (see Fig. S12-13 for further discussion).

The uptake data for all MOF samples can be fit to either the Lagergren pseudo-first-order (Eq S1) or pseudo-second-order (Eq S2) kinetic model as shown below.[S23] We note that such analysis is commonly used to probe for the presence of secondary processes. See further discussion in the caption of Fig. S13.

$$\log\left(q_e - q_t\right) = \log\left(q_e\right) - \frac{k_{s1}}{2.303}t$$
(S1)

$$\frac{t}{q_t} = \frac{1}{q_e}t + \frac{1}{k_{S2}q_e^2}$$
(S)

where:
t = time (min)
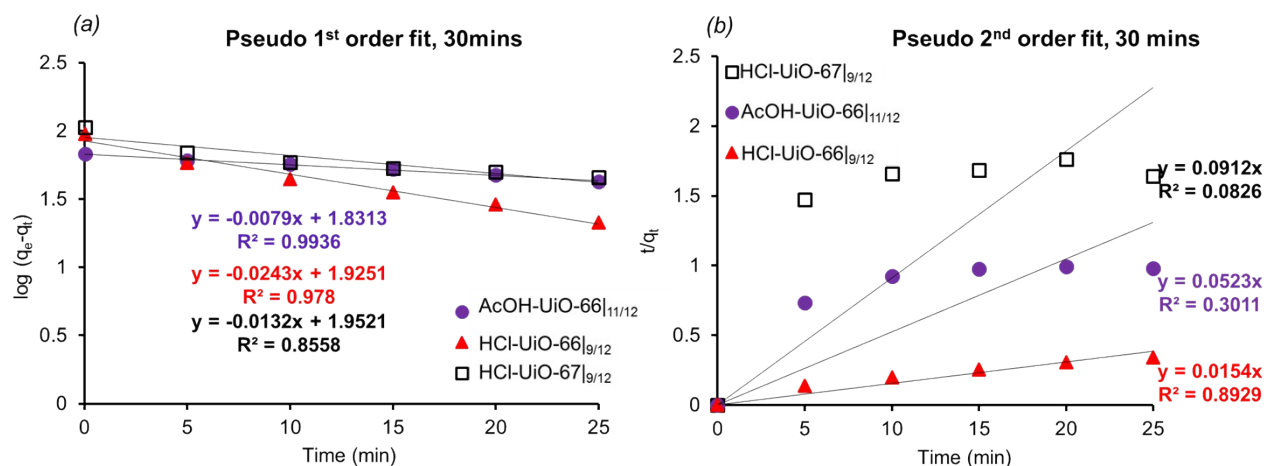q_e = equilibrium capacity (mg/g),
q_t = adsorbed quantity at a specific time (mg/g),
k_{S1} = pseudo first-order rate constant (min^{-1}), and
k_{S2} = pseudo second-order rate constant (g/(mg·min))

The corresponding data fits are shown in Figs. S12-S13 and the determined rate constants are listed in Table S3.

Fig. S12.   (a) Lagregren pseudo-first-order and (b) pseudo-second-order model fitting of the initial (within 30 mins) uptake data for samples of UiO-66 and analogues.   In all cases (including the other two HCl-UiO-66|$_{x/12}$ derivatives, data not shown), the Lagregren pseudo-first-order model provided the best fit to this initial uptake data.
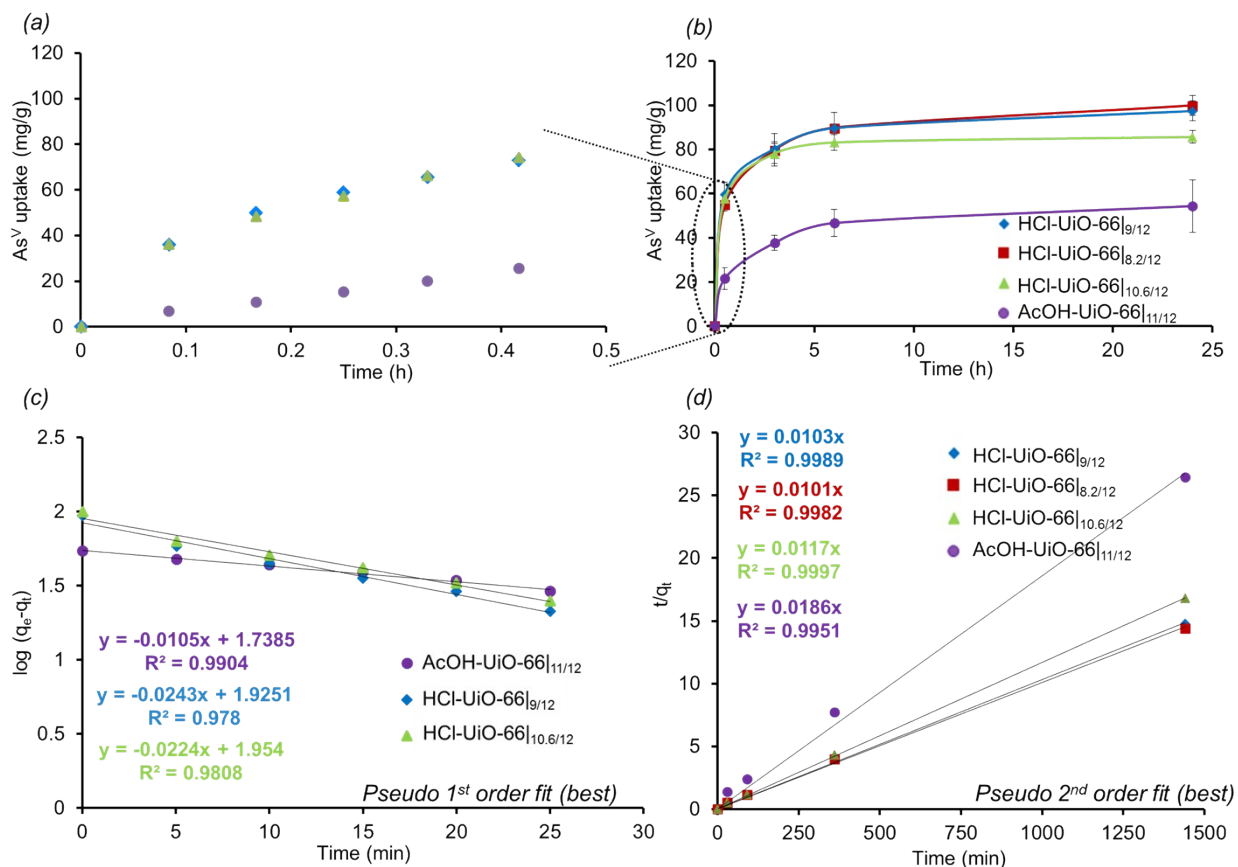
Fig. S13.   (a,b): The As^V-adsorption profiles for AcOH-UiO-66|$_{11/12}$ and the three HCl-UiO-66|$_{x/12}$ derivatives under conditions that favor the missing-linker-based uptake mechanism.   HCl-UiO-66|$_{x/12}$ samples with similar particle sizes (Fig. S6a) displayed similar initial (i.e., first 30 mins) uptake profiles (a) but diverge at longer times (b).   This divergence (i.e., starting at 3h with HCl-UiO-66|$_{10.6/12}$ having the lowest uptake) suggests that As^V-uptake capacity increases with larger amounts of defect density.   This is presumably due to the additional binding sites present and larger "average" internal spaces that facilitate As^V diffusion.   AcOH-UiO-66|$_{11/12}$, which have particle sizes that are 4 times as large (Fig. S6a), has a significantly slower initial uptake profile.   These observations suggest that both the particle size and defect density can play important roles in As^V

uptake but their relative contributions change at different stages of the adsorption. (c,d): The best fits of the adsoprtion profiles to the Lagregren pseudo-first-order (30 min uptake, c) and pseudo-second-order (24 h uptake, d) models. Similarly to that in Figure S11, the initial adsorption profiles for all four MOFs samples fit best to the pseudo-first-order model (bottom left panel) supports our hypothesis that initial uptake is mainly governed by chemisorption to the binding sites on the surface of the MOF particles. This conclusion is also consistent with literature findings[S23, 24] for Fe-BTC and other porous adsorbents for As^V. However, the total adsorption profiles over 24 h fit better to a pseudo-second-order model (bottom right panel), affirming the presence of a second, diffusion-limited process (i.e., binding to the accessible internal binding sites).

Table S3. Adsorption rates of As^V in UiO-66$|_{x/12}$ MOFs.

UiO-66 analogues	Rates	
	*Initial (30 min)	+Overall (1440 min)
AcOH-UiO-66$|_{11/12}$	1.50×10^{-2} min^{-1}	4.81×10^{-4} g/(mg·min)
HCl-UiO-66$|_{10.6/12}$	5.37×10^{-2} min^{-1}	1.29×10^{-4} g/(mg·min)
HCl-UiO-66$|_{9/12}$	5.27×10^{-2} min^{-1}	5.88×10^{-4} g/(mg·min)
HCl-UiO-66$|_{8.2/12}$	3.50×10^{-2} min^{-1}	4.49×10^{-4} g/(mg·min)

Calculated using Eqs S1* and S2+

**S7 Evidence of adsorption: DRIFTS, XPS, and TEM-EDS analyses**
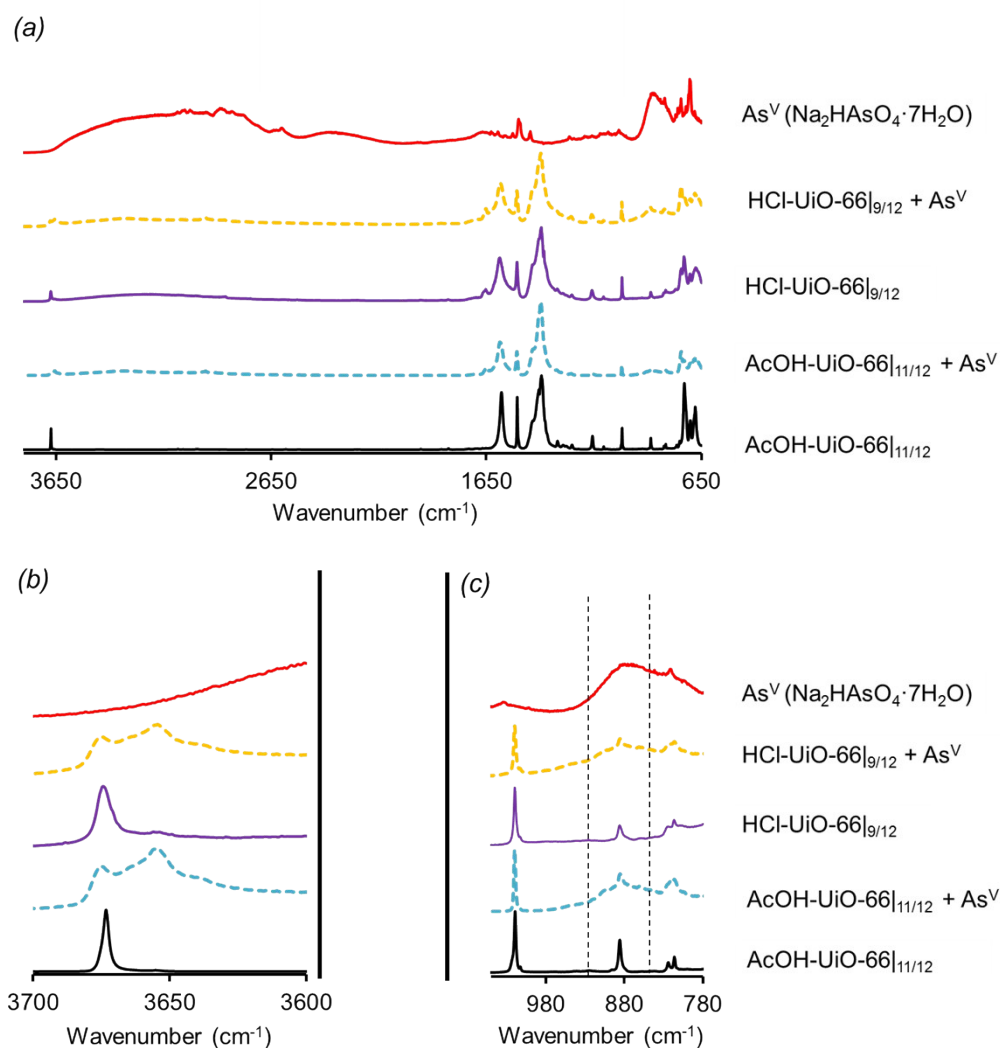
Fig. S14.   (a) DRIFT spectra of MOF samples before and after As^V treatment suggest successful As^V encapsulation. After As^V treatment (24 h of exposure to 30 mL of a solution of 50 ppm initial As^V concentration), samples were washed with DI water (2 × 30 mL) and acetone (1 × 30 mL) and activated at 120 ^oC overnight. (c) The broad stretch at ~880 cm^{-1}, which is attributed to As-O bonds,[S22, 25] appears in both As^V-treated MOF samples with an increased relative intensity in the HCl-UiO-66|$_{9/12}$ sample (top gold dotted plot). Additionally, the appearance of new peaks at the bridging hydroxide region (b, 3680-3630 cm^{-1}) in the DRIFT spectra of the MOFs after exposure to As^V suggest the presence of new As(OH) and AsO⋯H species that are similar to the As^V-O⋯H⋯OM species reported by Myneni *et al*,[S25] and the PO⋯H⋯OZr species reported by Deria *et al*.[S26]
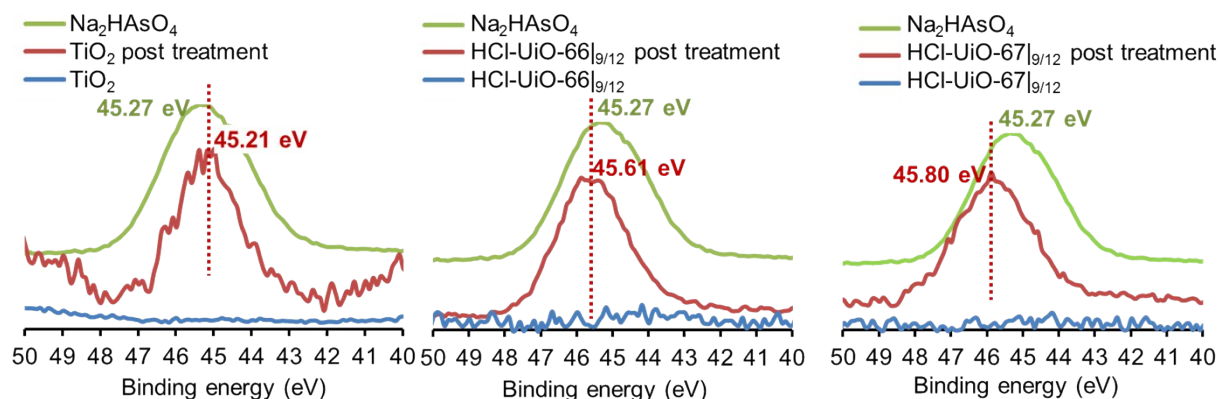
Fig. S15. As3d XPS spectra of MOFs and TiO_2 samples that have been exposed to a solution (30 mL) of 50 ppm initial As^V concentration for 24 h (i.e., at the point of highest As^V uptake in our study, see Fig. 3 in the main text). The XPS chemical shift for our As^V-exposed Ti sample is consistent with data previously obtained for As^V-TiO_2 surface complexation.[S27] Together with the data for the parent MOF before exposure and $Na_2HAsO_4 \cdot 7H_2O$, the data for the As^V-exposed MOF samples strongly support the presence of bound As^V. While it is tempting to note that the binding energies of As^V bound to the UiO analogues (middle and right spectra) are shited in a manner that is consistent with the increased presence of bound As^V (either Zr-O-As or As oligomers) in the MOF (by ~ 0.34 eV and ~ 0.53 eV for HCl-UiO-66|$_{9/12}$ and HCl-UiO-67|$_{9/12}$ respectively), these shifts are comparable to the ultimate resolution of our spectrometer (0.4 eV).
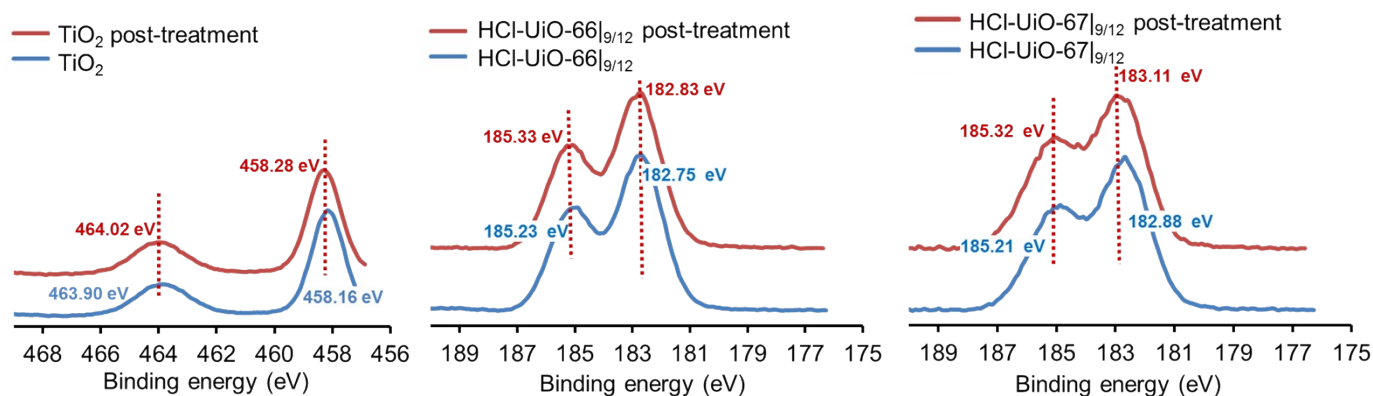
Fig. S16. Ti2p and Zr3d XPS spectra of the TiO_2. and MOFs, before and after As^V exposure (24 h of exposure to 30 mL of a solution of 50 ppm initial As^V concentration).
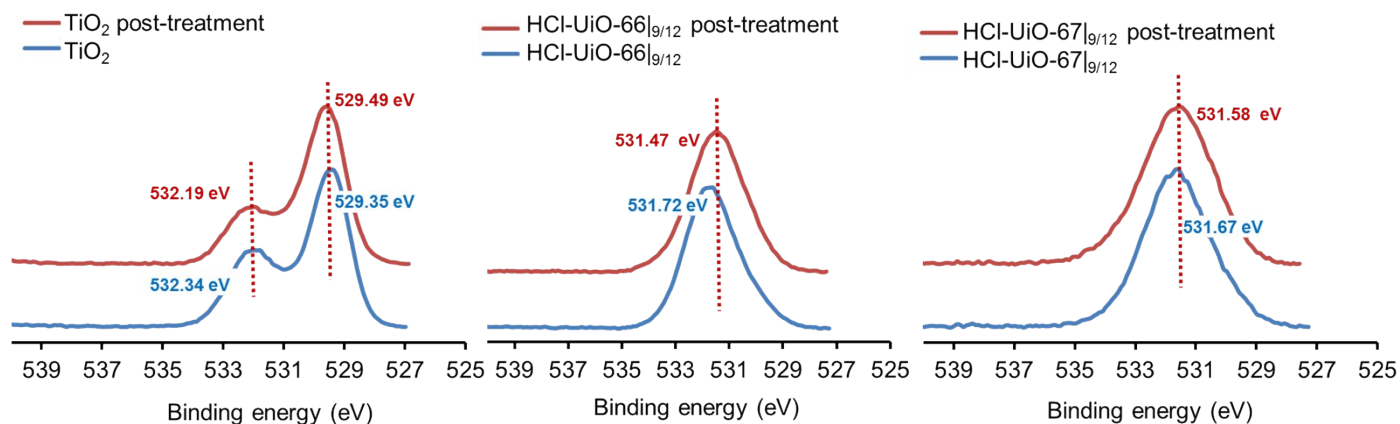

Fig. S17. O1s XPS spectra of the TiO_2 and MOFs, before and after As^V exposure (24 h of exposure to 30 mL of a solution of 50 ppm initial As^V concentration).
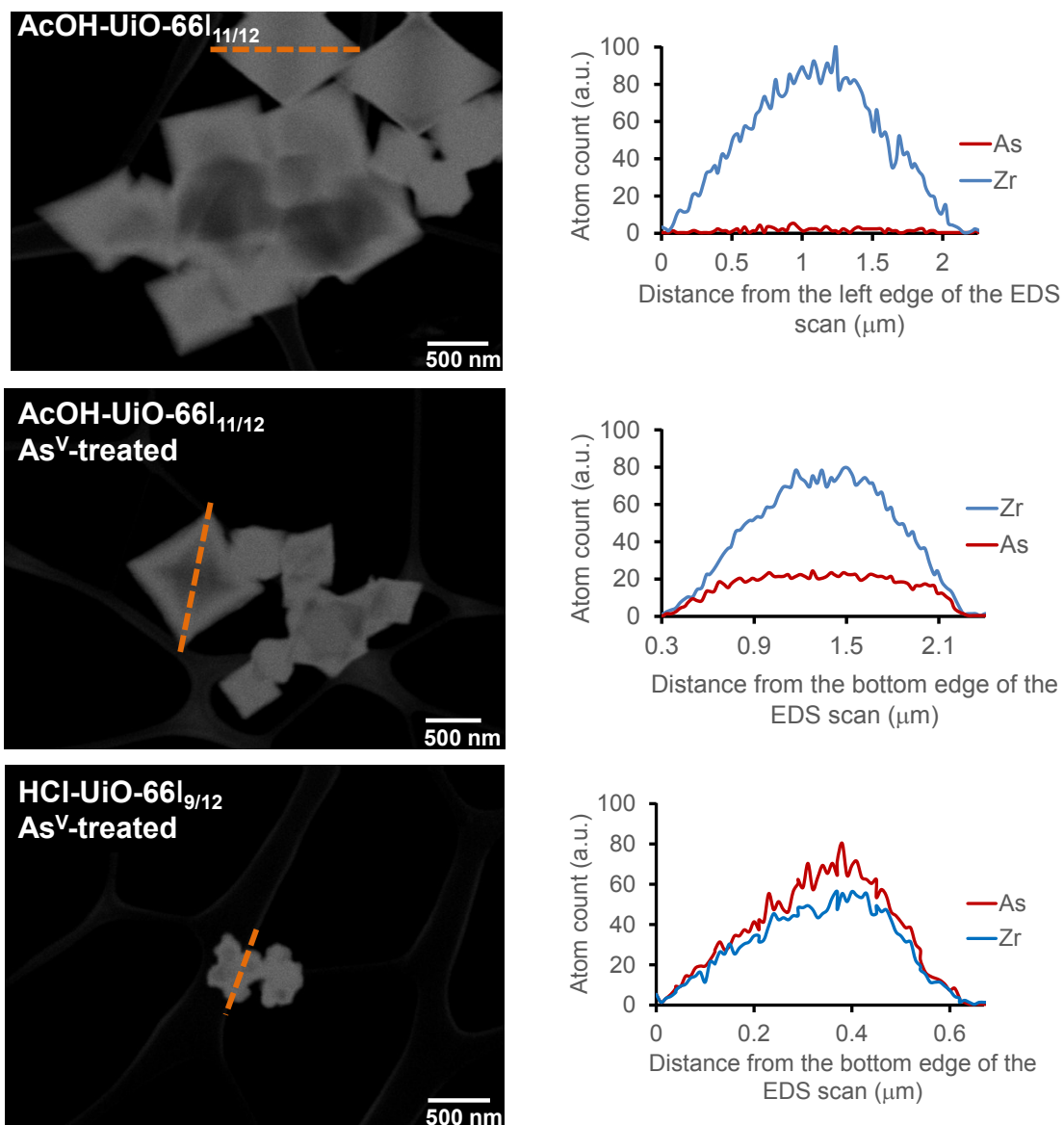
Fig. S18. Left panels: TEM images of AcOH-UiO-66|$_{11/12}$ exposed to water and AcOH-UiO-66|$_{11/12}$ and HCl-UiO-66|$_{9/12}$ exposed to As^V solution (30 mL of a solution of 100 ppm initial As^V concentration) for 24 hours. Right panels: The corresponding EDS linescans showing the amount of arsenic present with respect to zirconium. These data correspond to the scans that are traced by the orange dashed-lines in the images on the left.

S8. Other As$^{III/V}$ binding motifs possibilities
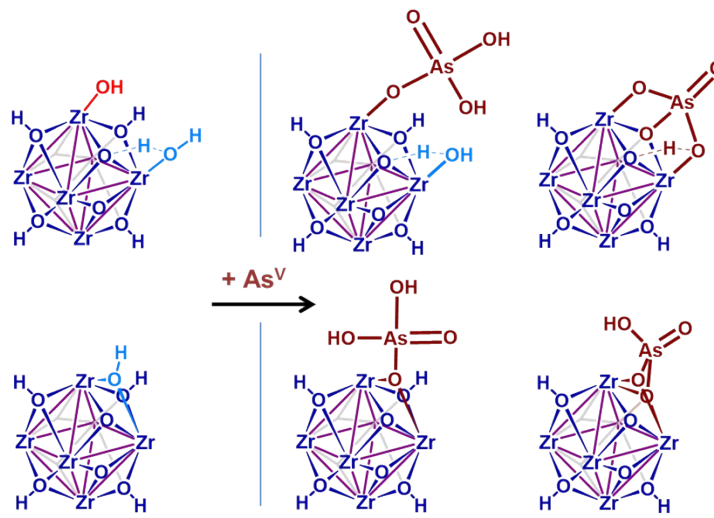
Fig. S19.   A schematic illustration showing other potential coordination motifs of As^V to the nodes of UiO-66 as the exact binding mode was not investigated by direct methods (e.g., pair distribution function). It is quite possible that some combinations of these binding modes will form rather than the energetically unfavorable displacement of the μ³-OH moiety.
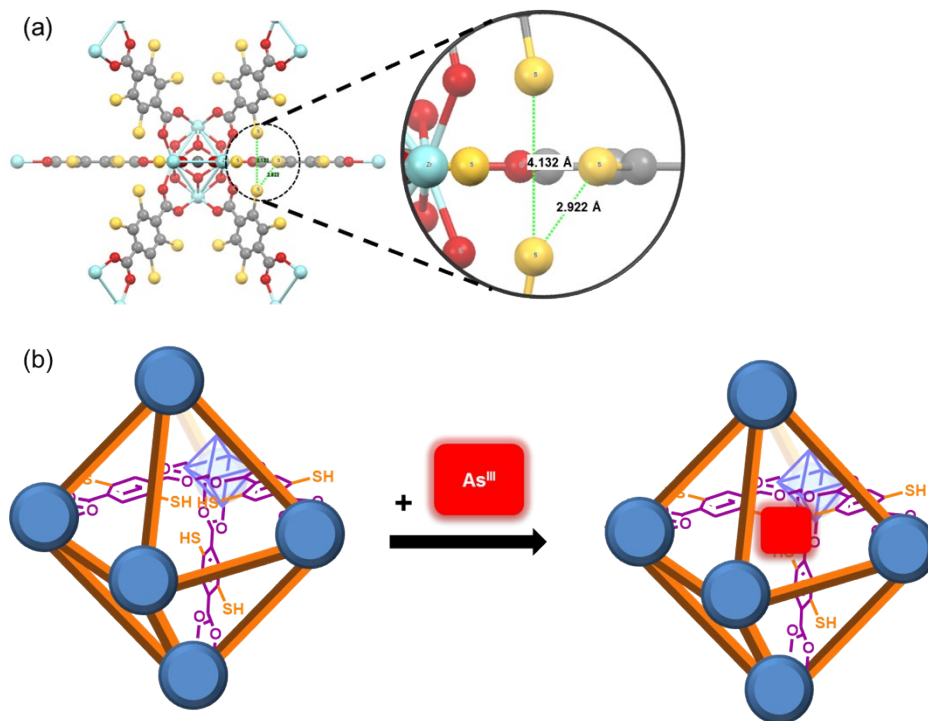
**Fig. S20**.   (a) A schematic representation[S20] of the node of UiO-66(SH)$_2$ where the linkers are shown to have four thiols (as opposed to two) due to potential rotational disorders in the simulated crystal structure. [S23] When the pre-oriented thiols are pointing into the same pore, the bond distances are close enough for synergistic complexation of As^{III}. (b) A schematic illustration showing the proposed binding motif for As^{III} in UiO-66(SH)$_2$. Note that while it may take ~2-3 rightly oriented thiols to bind one As^{III} in a strong, "chelated" fashion,[S28] some of the As^{III} may be bound more weakly through only one As-S linkage.
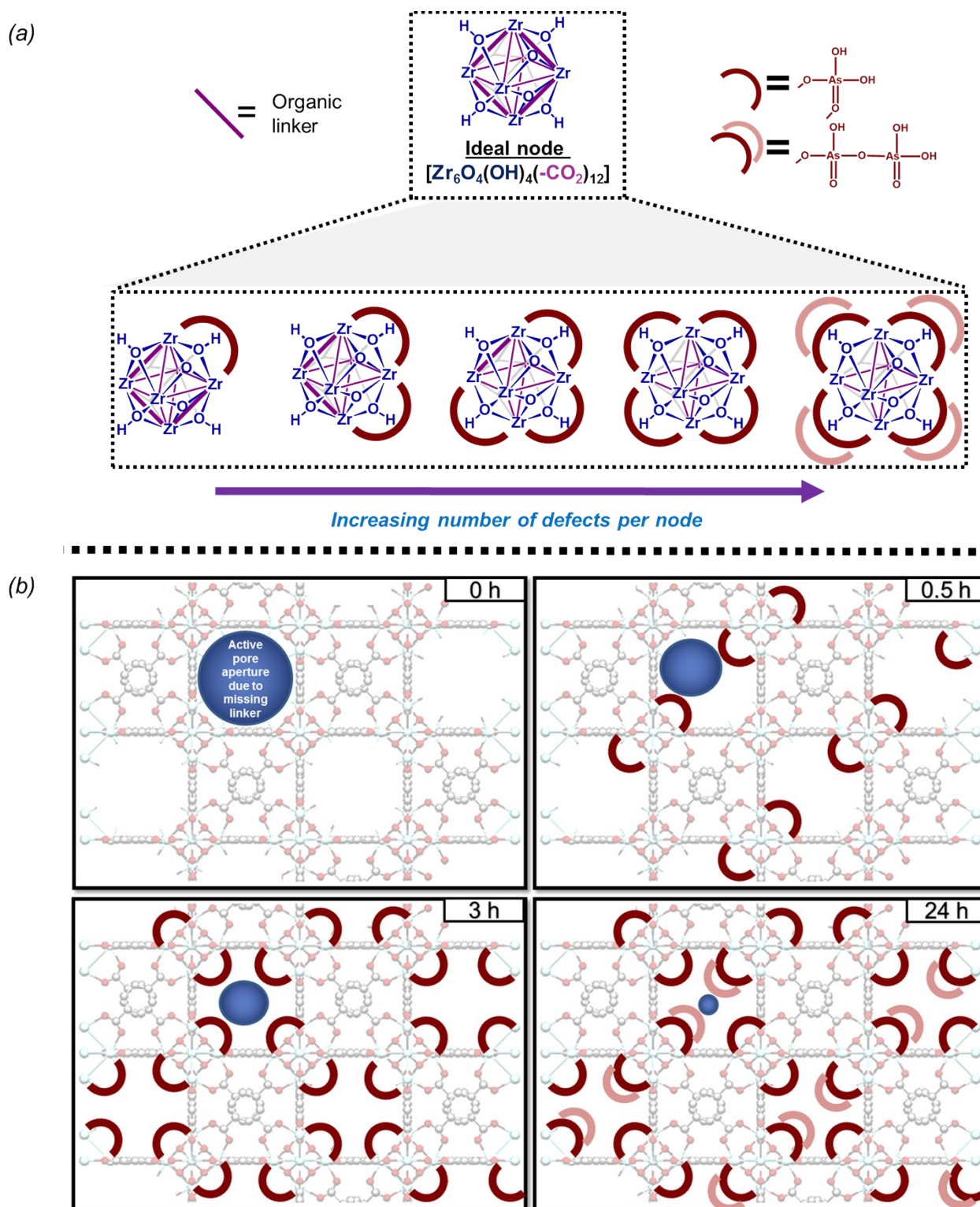
Fig. S21. (a) A schematic illustration of possible As^V-binding behavior to the defective nodes in HCl-UiO-66|$_{x/12}$ MOFs. (b) A perspective view into the first few layers of a MOF particle that is exposed to an As^V solution over time. As time passes, the pore aperture becomes more constricted, slowing down the diffusion rates of As^V ions into the internal binding sites.

S9. Arsenic desorption experiments

Regeneration of UiO-66 MOFs post-arsenate (As^V) treatment. The regeneration of MOF adsorbents with hexazirconium oxo hydroxo cluster nodes have been investigated after treatments with several oxyanions (i.e., phosphates,[S29] amino-bisphosphonates of alendronate,[S30] and sulfates[S31]). Lin and coworkers found that phosphate-treated UiO-66 could be partially regenerated (up to ~85% of the original capacity) by treatment a 1% NaCl solution.[S29] In a similar study, Shi and coworkers demonstrated that the release of amino-bisphosphonates of alendronate from UiO-66 could be expedited by increasing the acidity (pH 5.5 vs. pH 7.4) of the media at 37 ºC. These workers postulated that the release of this phosphonate-containing drug from the UiO-66 is most likely facilitated by the protonation of the phosphonate groups. As such we expected that the desorption of As^V oxyanions from As^V-treated AcOH-UiO-66|$_{11/12}$ and HCl-UiO-66|$_{9/12}$ samples is possible via simple ion-exchange chemistry (Eqs. 2a and b in the manuscript). See further discussion in the section entitled "The reversibility of As^{III} and As^V binding" in the manuscript. The relevant data and experimental conditions are summarized in Fig. S22 and Table S4 below.
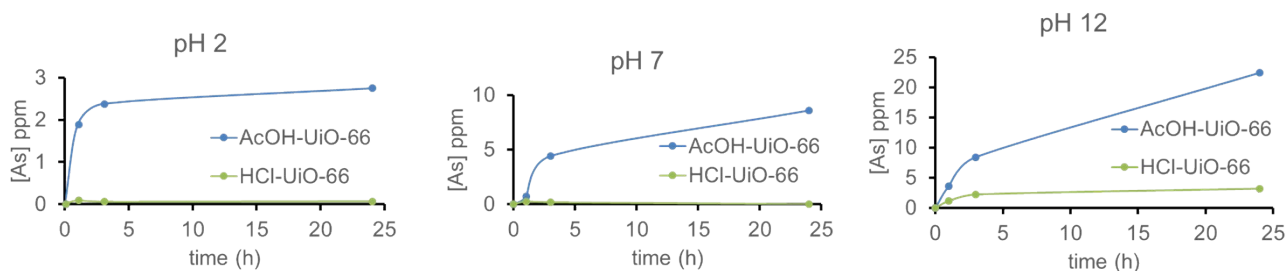
Fig. S22. Qualitative investigation of the effect of pH on the desorption of As^V. The plots show the amount of As desorbed, expressed as ppm concentrations in the supernatant, as a function of time in acidic, neutral, basic solutions. (Full desorption would yield 112 ppm for As^V-treated AcOH-UiO-66|$_{11/12}$ and 135 ppm for As^V-treated HCl-UiO-66|$_{9/12}$.) No Zr^{IV} ions leached out at pH 7 and 12, and only trace amounts (<1%) was found in the supernatant s after 24 h at pH 2. Experimental conditions: 50 mg of each As^V-treated UiO-66 sample was placed in a volume (30 mL) of un-buffered solution (pH = 2, 7, or 12), which was gently agitated using a Barnstead Thermolyne Labquake Shaker Rotisserie Model T400110 (Barnstead International, Dubuque, IA). ICP analysis was carried out on aliquots of the supernatant of the mixture after centrifuging at various time points.

Table S4. Tested desorption conditions for As^V-treated HCl-UiO-66|$_{9/12}$.

Approximate desorption agent/node ratio	% As desorbed	% of Zr^{IV} ions that leached from MOF sample	Desorption solution
15714 HCl/node	73	16	3.3M HCl (10 v/v % conc. HCl solution)*
5 HCl/node	0.3	0.008	0.015M HCl (pH = 1.8**)
10 HCl/node	0.6	0.02	0.03M HCl (pH = 1.5**)
5 NaOH/node	22	0.08	0.015M NaOH (pH = 12.2**)
10 NaOH/node	20	0.3	0.03M NaOH (pH = 12.5**)
1048 NaOH/node	93	2.7	3.3M NaOH
814 NaCl/node	5	0	1 wt % NaCl solution*

Experimental conditions: HCl-UiO-66|$_{9/12}$ was initially exposed to a As^V solution (32.5 mL of a 45 ppm As^V in water, pH 7) for 24 h to maintain a similar As:MOF ratio as in the batch treatments described in section S3. The remaining As concentration after exposure is ~18 ppm, which is comparable to those batch experiments. The MOF samples were then separated from the treatment solutions via centrifugation on a Spin-X centrifuge filter (product # 8161, Corning Inc., Corning, NY). The collected MOF samples were then exposed to the appropriate desorption solutions (2 mL except when noted), gently agitated for ~ 20 minutes, and then passed through a Spin-X centrifuge filter. Depending on the level of acidity and concentrations of the analyzed ions (pre-estimated from similar experiments), an appropriate amount of the filtrate were collected and analyzed by ICP-OES for As and Zr.
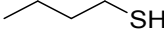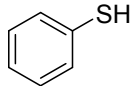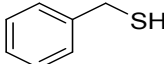**Exposed to 30 mL of desorption solution for 24 h.*
**Calculated values from concentration.

Regeneration of UiO-MOF post-arsenite (As^{III}) treatment. As most studies on arsenic removal generally focus on the removal of As^V, For applications where both As^{III} and As^V need to be removed, the As^{III} is routinely oxidized to As^V prior to adsorbent treatment. However, such treatment involves an extra oxidative step and can potentially oxidize the thiol

groups and/or the linker, rendering them unsuitable for reuse. Hence, we proposed that a simpler desorption process from using thiols ligand exchange (Eq. 1 in the manuscript). See further discussion in the section entitled "The reversibility of As^{III} and As^V binding" in the manuscript. The relevant data and experimental conditions are summarized in Table S5 below.

Table S5. Tested desorption conditions for As^{III}-treated HCl-UiO-66(SH)$_2$.

Thiols ligands (~90 equiv per node)	%As desorbed	% Zr^{IV} ions that leached from MOF sample**	% thiol ligands recovered**
⌁⌁⌁SH	11	0	20*
⬡SH	30	0	68
⬡SH	16	0	69

Experimental conditions: HCl-UiO-66(SH)$_2$ was initially exposed to an As^{III} solution (30 mL of 50 ppm As^{III} in water, pH 5) for 24 h at a similar As:MOF ratio as in the batch treatments described in section S3. The remaining As-concentration after exposure is ~35 ppm, which is comparable to those batch experiments. The MOF samples were then separated from the treatment solutions via centrifugation on a Spin-X centrifuge filter (product # 8161, Corning Inc., Corning, NY), resuspended in the appropriate desorption solutions (1 mL of a 0.486M thiol solution in EtOH), and stirred for 3 h at 50 °C. Note: heating and stirring are necessary for effective thiol exchange to occur. At room temperature and without stirring no As^{III} release was observed.

*We suspect that some of this butanethiol evaporated.

**Aliquots of the mixture (0.25 mL) were collected, digested in a small amount (2.5 mL) of a mixture of 6:3:1 v/v/v ratios of H_2O:conc. HNO_3:H_2O_2 (30 wt % in H_2O) inside an unsealed 2-5 mL microwave vial for 10 min at room temperature and then placed in a 70 °C preheated sand bath for ~ 8 h. The samples were then analyzed by ICP-OES for As, S, and Zr.

For the aforementioned studies, we attempted the regeneration in ethanol solution to maintain the solubility of the thiol ligands. Based on the % of As^{III} desorbed from As^{III}-treated HCl-UiO-66(SH)$_2$, it would appear that thiophenol is much better than alkylthiols at desorbing As^{III} from the MOFs. This is consistent with the ligand-exchange mechanism described in Eq. 1 in the manuscript where the exchange is thermodynamically favored with the more reactive thiophenol (pK$_a$ = 6.6) in comparison to benzyl mercaptan (pK$_a$ = 9.4) and butane thiol (pK$_a$ =10.8).

S10. Miscellaneous calculations

For the most defective HCl-UiO-66|$_{9/12}$ MOF derivative, with a molecular formula of Zr$_6$O$_4$(OH)$_4$(linker)$_{4.5}$Cl$_3$(H$_2$O)$_3$ (each missing carboxylate is assumed to be replaced by a Cl ion and a water molecule), exposure to 30 mL of a 50 ppm As (0.02 mmol As) affords a slight excess of arsenic in solution in comparison to the binding sites (i.e., defect sites). This amount is still in excess for the less defective AcOH-UiO-66|$_{11/12}$ MOF, the less dense HCl-UiO-67|$_{9/12}$, or the denser HCl-UiO-66(SH)$_2$ and AcOH-UiO-66(SH)$_2$ (both of which are also less defective). The calculations are as follows:

10 mg of HCl-UiO-66|$_{9/12}$ (MW = 1578.3 g/mol) = 0.0063 mmol Zr$_6$, which equate to a 1:3.17 Zr$_6$:As
10 mg of AcOH-UiO-66|$_{11/12}$ (MW = 1641.06 g/mol) = 0.0061 mmol Zr$_6$, which equate to a 1:3.27 Zr$_6$:As
10 mg of HCl-UiO-67|$_{9/12}$ (MW = 1920.78 g/mol) = 0.0052 mmol Zr$_6$, which equate to a 1:3.84 Zr$_6$:As
10 mg of HCl-UiO-66(SH)$_2$|$_{10.5/12}$ (MW = 1957.85 g/mol) = 0.0051 mmol Zr$_6$, which equate to a 1:3.92 Zr$_6$:As
10 mg of AcOH-UiO-66(SH)$_2$|$_{10.5/12}$ (MW = 1966.20 g/mol) = 0.0051 mmol Zr$_6$, which equate to a 1:3.93 Zr$_6$:As
10 mg of HCl-UiO-66(OH)$_2$|$_{12/12}$ (MW = 1856.10 g/mol) = 0.0054 mmol Zr$_6$, which equate to a 1:3.71 Zr$_6$:As
10 mg of ideal UiO-66 (MW = 1564.08 g/mol) = 0.0060 mmol Zr$_6$, which equate to a 1:3.33 Zr$_6$:As
10 mg of ideal UiO-66(SH)$_2$ (MW = 2048.82 g/mol) = 0.0049 mmol Zr$_6$, which equate to a 1:4.08 Zr$_6$:As

S11. Author contributions audits

data analysis. O.K.F, J.T.H., and S.T.N. supervised the project. C.O.A. wrote the initial drafts of the paper. C.O.A. and S.T.N. finalized the manuscript with inputs from all co-authors.

S12. References

S1. L. Vial, R. F. Ludlow, J. Leclaire, R. Pérez-Fernández and S. Otto, *J. Am. Chem. Soc.*, 2006, **128**, 10253-10257.

S2. B. C. Lippens and J. H. de Boer, *J. Catal.*, 1965, **4**, 319-323.

S3. S. Chakraborty, Y. J. Colon, R. Q. Snurr and S. T. Nguyen, *Chem. Sci.*, 2015, **6**, 384-389.

S4. A. W. Marczewski, *http://adsorption.org/awm/ads/meso/RIB-ASAP.htm*, Accessed January 5, 2016.

S5. *http://www.micromeritics.com/Product-Showcase/MicroActive-Interactive-Data-Analysis-Software/MicroActive-Interactive-Data-Analysis-Reports.aspx*, Accessed January 5, 2016.

S6. P. Li, R. C. Klet, S.-Y. Moon, T. C. Wang, P. Deria, A. W. Peters, B. M. Klahr, H.-J. Park, S. S. Al-Juaid, J. T. Hupp and O. K. Farha, *Chem. Commun.*, 2015, **51**, 10925-10928.

S7. These reported % yields are not accurate as these MOFs can trap a significant amount of solvent and water inside their pores.

S8. C. Wang, X. Liu, J. P. Chen and K. Li, *Sci. Rep.*, 2015, **5**, 16613/16611-16610.

S9. K. A. Kercher and C. D. Nagle, *Wood Sci. Technol.*, 2001, **35**, 325-341.

S10. A. Gomez-Caminero, P. Howe, M. Hughes, E. Kenyon, D. R. Lewis, M. Moore, J. Ng, A. Aitio and G. Becking., *Arsenic and Arsenic compounds [Online]*, 2nd ed., International Programme on Chemical Safety, WHO, Geneva, 2001. Section 3.1. http://www.inchem.org/documents/ehc/ehc/ehc224.htm#3.1 (accessed May 27, 2016).

S11. C. W. Abney, K. M. L. Taylor-Pashow, S. R. Russell, Y. Chen, R. Samantaray, J. V. Lockard and W. Lin, *Chem. Mater.*, 2014, **26**, 5231-5243.

S12. J. E. Mondloch, M. J. Katz, N. Planas, D. Semrouni, L. Gagliardi, J. T. Hupp and O. K. Farha, *Chem. Commun.*, 2014, **50**, 8944-8946.

S13. J. B. DeCoste, G. W. Peterson, B. J. Schindler, K. L. Killops, M. A. Browe and J. J. Mahle, *J. Mater. Chem. A*, 2013, **1**, 11922-11932.

S14. M. J. Katz, Z. J. Brown, Y. J. Colon, P. W. Siu, K. A. Scheidt, R. Q. Snurr, J. T. Hupp and O. K. Farha, *Chem. Commun.*, 2013, **49**, 9449-9451.

S15. P. Ghosh, Y. J. Colon and R. Q. Snurr, *Chem. Commun.*, 2014, **50**, 11329-11331.

S16. H. G. T. Nguyen, N. M. Schweitzer, C. Y. Chang, T. L. Drake, M. C. So, P. C. Stair, O. K. Farha, J. T. Hupp and S. T. Nguyen, *ACS Catal.*, 2014, **4**, 2496-2500.

S17. G. C. Shearer, S. Chavan, J. Ethiraj, J. G. Vitillo, S. Svelle, U. Olsbye, C. Lamberti, S. Bordiga and K. P. Lillerud, *Chem. Mater.*, 2014, **26**, 4068-4071.

S18. L. Valenzano, B. Civalleri, S. Chavan, S. Bordiga, M. H. Nilsen, S. Jakobsen, K. P. Lillerud and C. Lamberti, *Chem. Mater.*, 2011, **23**, 1700-1718.

S19. H. Wu, Y. S. Chua, V. Krungleviciute, M. Tyagi, P. Chen, T. Yildirim and W. Zhou, *J. Am. Chem. Soc.*, 2013, **135**, 10525-10532.

S20. K. K. Yee, N. Reimer, J. Liu, S. Y. Cheng, S. M. Yiu, J. Weber, N. Stock and Z. Xu, *J. Am. Chem. Soc.*, 2013, **135**, 7795-7798.

S21. As^{III} adsorption was carried out at pH 5 to facilitate the conversion of two As-OH moieties on arsenite into stable chelating As-SR bonds as shown in the reaction of thiol-rich proteins with Lewisite (L. A. Stocken and R. H. S. Thompson, *Biochem J.*, 1946, **40**, 529-535.)

S22. J. A. Tossell, *Geochim. Cosmochim. Acta*, 1997, **61**, 1613-1623.

S23. Y. S. Ho and G. McKay, *Process Biochem.*, 1999, **34**, 451-465.

S24. B.-J. Zhu, X.-Y. Yu, Y. Jia, F.-M. Peng, B. Sun, M.-Y. Zhang, T. Luo, J.-H. Liu and X.-J. Huang, *J. Phys. Chem. C*, 2012, **116**, 8601-8607.

S25. S. C. B. Myneni, S. J. Traina, G. A. Waychunas and T. J. Logan, *Geochim. Cosmochim. Acta*, 1998, **62**, 3499-3514.

S26. P. Deria, W. Bury, I. Hod, C.-W. Kung, O. Karagiaridi, J. T. Hupp and O. K. Farha, *Inorg. Chem.*, 2015, **54**, 2185-2192.

S27. S. Bang, M. Patel, L. Lippincott and X. Meng, *Chemosphere*, 2005, **60**, 389-397.

S28. A. M. Spuches, H. G. Kruszyna, A. M. Rich and D. E. Wilcox, *Inorg. Chem.*, 2005, **44**, 2964-2972.

S29. K.-Y. A. Lin, S.-Y. Chen and A. P. Jochems, *Mater. Chem. Phys.*, 2015, **160**, 168-176.

S30. X. Zhu, J. Gu, Y. Wang, B. Li, Y. Li, W. Zhao and J. Shi, *Chem. Commun.*, 2014, **50**, 8779-8782.

S31. A. J. Howarth, T. C. Wang, S. S. Al-Juaid, S. G. Aziz, J. T. Hupp and O. K. Farha, *Dalton Trans.*, 2016, **45**, 93-97.